Cell Reports

Article

Defective extracellular matrix remodeling in brown adipose tissue is associated with fibro-inflammation and reduced diet-induced thermogenesis

Graphical abstract

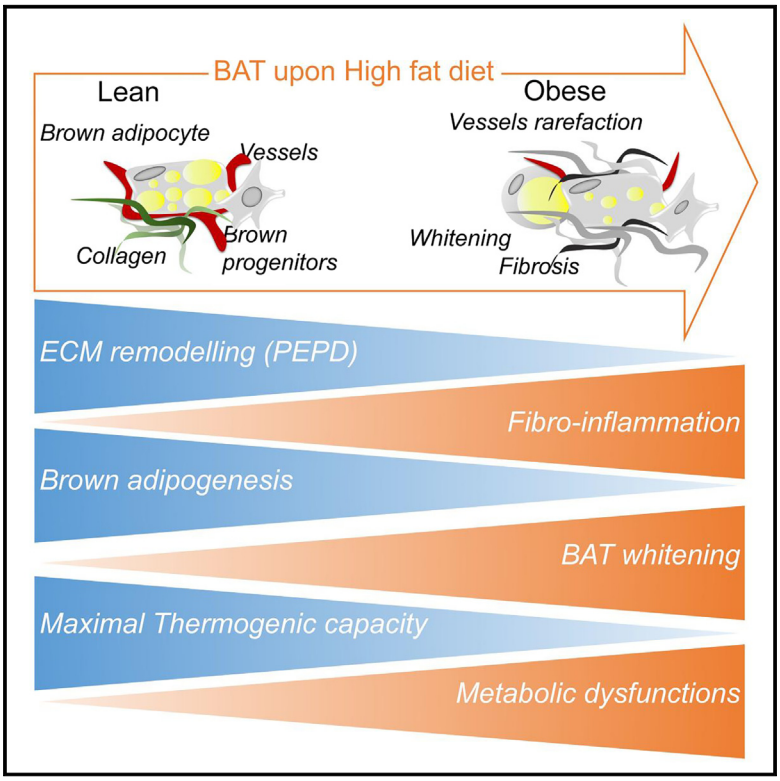

Highlights

- HFD causes BAT fibro-inflammation and impairs the maximal thermogenic capacity
- Fibro-inflammatory environment impairs brown adipocyte functions
- Inactivated BAT features fibro-inflammation in mice and humans
- *Pepd* partial ablation exacerbates BAT dysfunction and fibro-inflammation induced by HFD

Authors

Vanessa Pellegrinelli, Elizabeth Figueroa-Juárez, Isabella Samuelson, ..., Stefania Carobbio, Kirsi A. Virtanen, Antonio Vidal-Puig

Correspondence

vp332@medschl.cam.ac.uk (V.P.), ajv22@medschl.cam.ac.uk (A.V.-P.)

In brief

Pellegrinelli et al. show that obesity induces BAT fibro-inflammation associated with impaired BAT maximal thermogenic capacity in mice and reduced BAT activity in humans. The study highlights the relevance of the ECM remodeling-associated protein, PEPD, in BAT fibro-inflammation and function in response to temperature challenges and HFD.

Pellegrinelli et al., 2023, Cell Reports *42*, 112640
June 27, 2023
https://doi.org/10.1016/j.celrep.2023.112640

CellPress

Cell Reports

CellPress
OPEN ACCESS

Article

Defective extracellular matrix remodeling in brown adipose tissue is associated with fibro-inflammation and reduced diet-induced thermogenesis

Vanessa Pellegrinelli,[1,*] Elizabeth Figueroa-Juárez,[1,14] Isabella Samuelson,[1,14] Mueez U-Din,[2,3] Sonia Rodriguez-Fdez,[1] Samuel Virtue,[1] Jennifer Leggat,[1] Cankut Çubuk,[4] Vivian J. Peirce,[1] Tarja Niemi,[5] Mark Campbell,[1,6] Sergio Rodriguez-Cuenca,[1,6] Joaquin Dopazo Blázquez,[4,7,8,9] Stefania Carobbio,[1,10] Kirsi A. Virtanen,[2,11,12] and Antonio Vidal-Puig[1,6,10,13,15,*]

[1]Wellcome-MRC Institute of Metabolic Science and Medical Research Council Metabolic Diseases Unit, University of Cambridge, Cambridge, UK
[2]Turku PET Centre, University of Turku, Turku, Finland
[3]Turku PET Centre, Turku University Hospital, Turku, Finland
[4]Platform of Computational Medicine, Fundación Progreso y Salud (FPS), Hospital Virgen Del Rocío, 41013 Sevilla, Spain
[5]Department of Plastic and General Surgery, Turku University Hospital, Turku, Finland
[6]Cambridge University Nanjing Centre of Technology and Innovation, Nanjing, P.R. China
[7]Bioinformatics in RareDiseases (BiER), Centro de Investigación Biomédica en Red de Enfermedades Raras (CIBERER), 41013 Sevilla, Spain
[8]Computational Systems Medicine, Institute of Biomedicine of Seville (IBiS), Sevilla 41013, Spain
[9]Functional Genomics Node (INB-ELIXIR-es), Sevilla, Spain
[10]Centro de Investigacion Principe Felipe (CIPF), Valencia, Spain
[11]Institute of Public Health and Clinical Nutrition, University of Eastern Finland (UEF), Kuopio, Finland
[12]Department of Endocrinology and Clinical Nutrition, Kuopio University Hospital, Kuopio, Finland
[13]Cambridge Heart and Lung Research Institute, Cambridge, UK
[14]These authors contributed equally
[15]Lead contact
*Correspondence: vp332@medschl.cam.ac.uk (V.P.), ajv22@medschl.cam.ac.uk (A.V.-P.)
https://doi.org/10.1016/j.celrep.2023.112640

SUMMARY

The relevance of extracellular matrix (ECM) remodeling is reported in white adipose tissue (AT) and obesity-related dysfunctions, but little is known about the importance of ECM remodeling in brown AT (BAT) function. Here, we show that a time course of high-fat diet (HFD) feeding progressively impairs diet-induced thermogenesis concomitantly with the development of fibro-inflammation in BAT. Higher markers of fibro-inflammation are associated with lower cold-induced BAT activity in humans. Similarly, when mice are housed at thermoneutrality, inactivated BAT features fibro-inflammation. We validate the pathophysiological relevance of BAT ECM remodeling in response to temperature challenges and HFD using a model of a primary defect in the collagen turnover mediated by partial ablation of the *Pepd* prolidase. *Pepd*-heterozygous mice display exacerbated dysfunction and BAT fibro-inflammation at thermoneutrality and in HFD. Our findings show the relevance of ECM remodeling in BAT activation and provide a mechanism for BAT dysfunction in obesity.

INTRODUCTION

Brown adipose tissue (BAT) has high metabolic activity and can be activated to improve glucose and lipid uptake and energy expenditure (EE), making it a promising target for treating cardio-metabolic disease.[1] Recent advancements in detecting and measuring BAT mass and activity have challenged the idea that obesity causes BAT loss and dysfunction.[2,3] However, obese individuals generally have lower levels of BAT mass and a smaller proportion of activated BAT in response to cold, suggesting that obesity may worsen BAT mass and function.[3,4] In obese mice, BAT is inflamed and infiltrated with macrophages,[5–7] but it is unclear if BAT inflammation is associated with fibrosis, as observed in white adipose tissue (WAT)[8] and whether fibro-inflammation limits BAT activation. Here, we investigate the hypothesis that BAT's defective extracellular matrix (ECM) remodeling in the context of physiological and pathophysiological conditions modulates BAT recruitment and function.

The ECM is crucial for adipose tissue (AT), providing structure and regulating biological functions (differentiation, hypertrophy, proliferation), and allowing intercellular communication.[9,10] Efficient ECM remodeling depends on its components' integrity (e.g., collagens, elastin, fibronectin), the functionality of ECM receptors, such as integrins,[9] as well as the coordinated regulation of biosynthesis and degradation mediated by growth factors

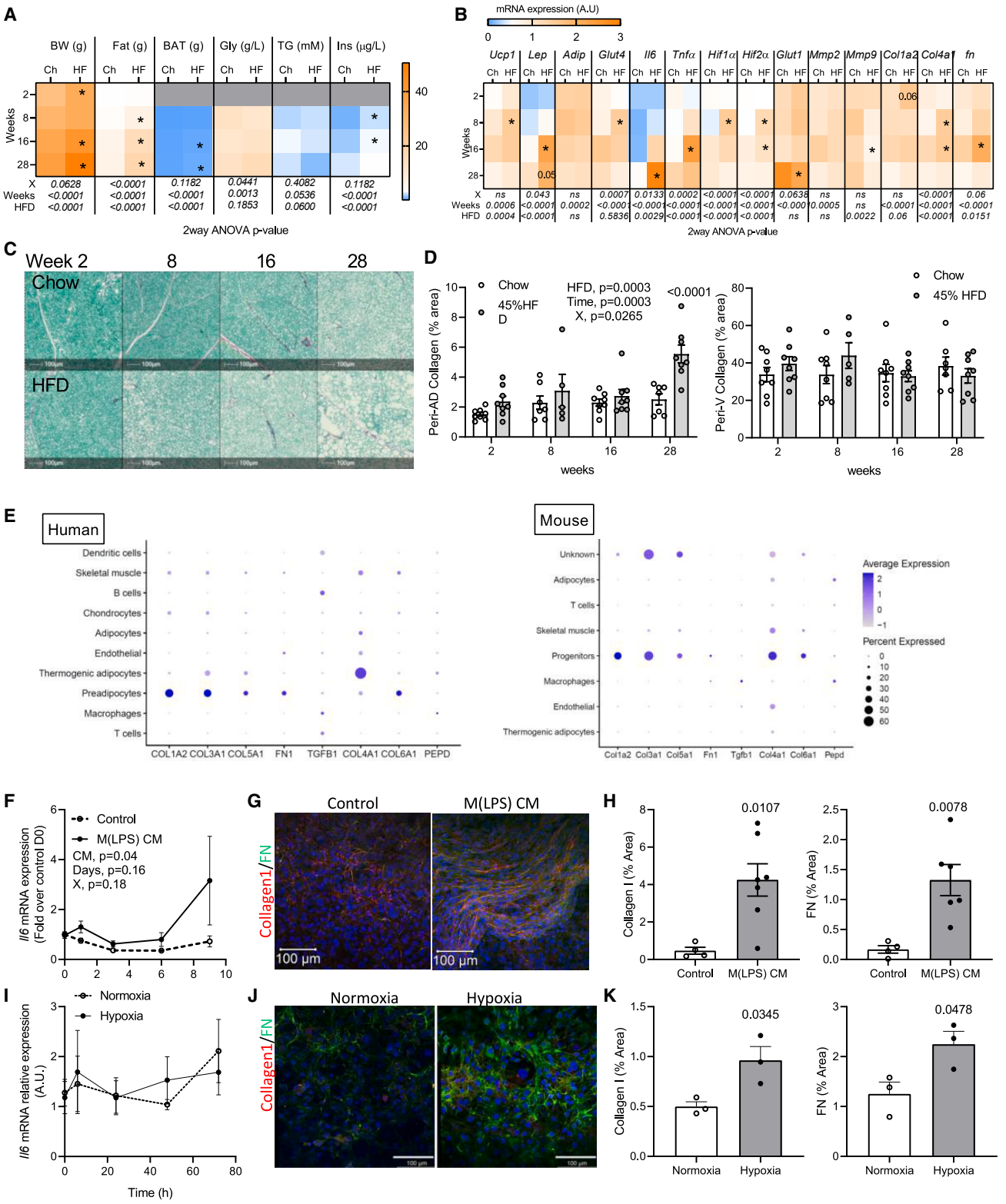

Figure 1. Long-term HFD exposure induces BAT fibro-inflammation

(A and B) Heatmap of metabolic parameters (including glycemia [gly], triglycerides [TG], and insulinemia [ins]) (A) and mRNA expression of metabolic and fibro-inflammatory marker (B) from C57Bl/6 mice fed 2, 8, 16, or 28 weeks (n = 8/group) with chow diet (Ch) or HFD 45% (HF).

(legend continued on next page)

(e.g., CTGF, TGF-β) and enzymes (e.g., matrix metalloproteinases MMP2, MMP9, and MMP14 and the intracellular peptidase D, among others[11,12]), respectively. Chronic inflammation in obesity-related diseases can lead to tissue fibrosis, a pathological outcome resulting from an imbalance of ECM remodeling that leads to excessive accumulation of fibrotic collagens (e.g., collagen 1, 3, and 6).[13]

Obesity is associated with WAT fibro-inflammation, which impairs tissue function and is associated with whole-body insulin resistance.[8,14–16] However, the role of ECM in BAT function and regulation in response to obesity is not well understood. Pharmacological activation of thermogenesis *in vitro* induces the expression and secretion of ECM components,[17,18] and some ECM components (i.e., laminin α4[19] and hyaluronan[20]) are relevant in regulating BAT/brown adipocyte thermogenic activity. Several observations suggest that an excess of ECM in BAT (i.e., fibrosis) might impair BAT functionality. For instance, endotrophin, a secreted cleavage product of COL6A3, is an effector of metabolic dysfunction, inflammation, and fibrosis in BAT.[21] Additionally, blocking vascular endothelial growth factor (VEGF) signaling in mice led to excess collagen I deposition, increased macrophage infiltration, and increased brown adipocyte death in BAT.[22]

The relationship between obesity and dysregulated ECM in BAT is of significant interest. Obesity-induced whitening and dysfunction of BAT are well described.[5,23–27] However, whether BAT ablation or dysfunction can lead to obesity is still debated because studies using models of BAT whitening (using thermoneutrality [TN] or targeting the uncoupling protein UCP1) have yielded paradoxical results, not showing a systematically associated weight gain.[28–32]

Using a combination of human and murine models of BAT activation/atrophy, obesity, and unbalanced ECM remodeling (i.e., *Pepd*-ablated animals), we show that ECM remodeling is essential to sustain BAT activation. We also show that obesity-related fibro-inflammation compromises BAT ECM remodeling and functionality, contributing to obesity-associated metabolic disturbances.

RESULTS

Long-term HFD exposure induces BAT fibro-inflammation

We investigated the occurrence of fibro-inflammation in BAT in response to a high-fat diet (HFD), a pathological proinflammatory context paradoxically associated with BAT activation (diet-induced thermogenesis).[33] We assessed BAT fibrosis and functions at 2, 8, 16, and 28 weeks of HFD. We validated that HFD-fed mice showed increased body weight (BW), fat mass, and insulinemia during the course of HFD and compared with chow-fed mice (Figure 1A). The most characteristic event after two weeks on HFD was the enhanced vascularization in BAT (Figure S1A). In line with diet-induced thermogenesis,[34] *Ucp1* mRNA expression increased in response to HFD, followed by increased lipid droplet accumulation in BAT at eight weeks of HFD at significantly higher levels than in chow-fed mice (Figures 1B, S1B, and S1C). BAT whitening was associated with higher expression of *Hif1α*, *Hif2α*, and *col4a1*. By 16 weeks on HFD, *Ucp1* expression was similar in chow and HFD-fed mice (Figure 1B). This convergence in *Ucp1* mRNA levels between chow and HFD coincided with the whitening of BAT (increased *leptin* expression), increased inflammation, higher BW and BAT mass, and exacerbation of metabolic complications, including liver steatosis and hyperinsulinemia (Figures 1A, 1B, S1D and S1E). After 16 weeks on HFD, gene expression levels of *Tnfα* in BAT were increased, suggesting the recruitment of macrophages (Figure 1B), as previously described in DIO models.[27] *Col4a1* and *Fn* expression was also increased, and *Mmp9* decreased compared with chow conditions, suggesting an imbalance of ECM remodeling in long-term HFD conditions (Figure 1B). The histological analysis revealed a significant increase in peri-adipocyte (peri-AD) collagen accumulation after 28 weeks of HFD, coinciding with higher *Il6* expression in BAT than in chow conditions (Figures 1B–1D). This suggests a connection between BAT fibrosis and inflammation. These data suggest that BAT is susceptible to fibro-inflammation in response to long-term HFD feeding, similar to what is observed in WAT.

We then investigated which cells were responsible for BAT ECM production and remodeling. We reanalyzed mouse and human BAT single-nucleus RNA sequencing (RNA-seq) (GEO: GSE202630[35] and EBI: E-MTAB-8564[36]). Both human and murine data show that collagen 1, 3, and 5 are mainly expressed in BAT progenitors/preadipocytes, while collagen 4 expression is shared among adipocytes, endothelial cells, and progenitors (Figure 1E). These results are confirmed by our gene expression analysis performed in murine BAT. Our analysis showed that brown adipocyte progenitors (BAPs) expressed 80% of collagen 1 and 6, while collagen 4 expression was shared among BAPs (30%), endothelial cells (36%), and mature adipocytes (15%) (Figure S2A). *Pepd*, coding for the intracellular protease promoting collagen degradation and turnover,[12] was primarily expressed by mature brown adipocytes and

(C and D) Representative images of red Sirius staining in BAT from C57Bl/6 mice fed 2, 8, 16, or 28 weeks (n = 8/group) with chow diet or HFD 45% (C) and corresponding quantification of peri-adipocyte (peri-AD) and peri-vascular (peri-V) collagen deposition represented as percentage tissue area (D). Scale bar: 100 μm.

(E–K) Dot plot showing expression of ECM/ECM marker genes in human (deep neck) and murine (interscapular) BAT. (F and I) mRNA expression of *il6* during time course differentiation of C57BAT (F) or pBAT (I) cells cultured with conditioned medium from LPS-stimulated bone marrow-derived macrophages (BMDMs) (M [LPS] CM) compared with control (F) or cultured in hypoxia condition (5% O_2) compared with normoxia (21% O_2) (I). n = 6/condition. (G, H, J, and K) Representative images of confocal analysis of anti-collagen type I (in red) and fibronectin (in green) in C57BAT (G) or pBAT (J) cells cultured with M(LPS) CM compared with control (G) or cultured in hypoxia condition (5% O_2) compared with normoxia (21% O_2) (J) and respective quantification (H and K). n = 6/condition. Scale bar: 100 μm.

Data are presented as mean ± SEM. One-way ANOVA with Šidák's post hoc multiple-comparisons test was used to compare with week 2 HFD in chow or HFD (A and B). Two-way ANOVA with Šidák's post hoc multiple-comparisons test was used to compare chow and HFD-fed mice (D) or day 9 with day 0 in control and M(LPS) CM conditions (D, F, and I). Student's t test was used to compare control/M(LPS) CM and normoxia/hypoxia conditions (H and K).

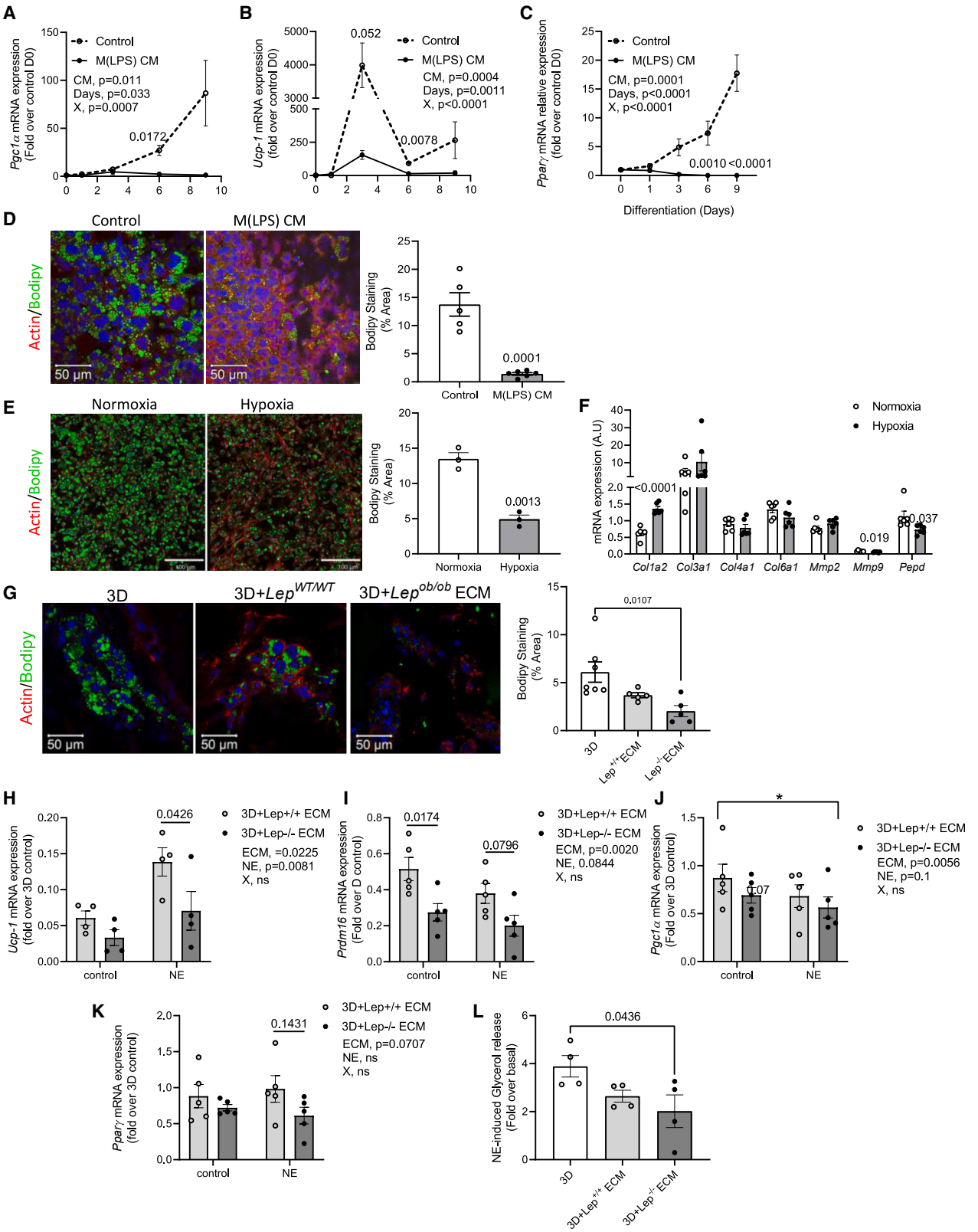

(legend on next page)

macrophages, as previously described[37] (Figures 1E and S2A). Interestingly, the relevance of the stromal vascular fraction (SVF) in expressing ECM/ECM remodeling markers was retained in BAT from obese mice (Figure S2B).

In WAT, fibrosis deposition has been associated with hypoxia and unresolved inflammation.[8] Given the higher expression of hypoxic and inflammatory markers in BAT from obese mice, we investigated if hypoxic and inflammatory environments regulated ECM production from BAPs. First, BAPs (brown preadipocyte cell line[38]) were differentiated in the presence of conditioned medium (CM) produced from proinflammatory macrophages (lipopolysaccharide [LPS]-treated macrophages [M(LPS) CM]) (figure S3A). As expected, BAPs significantly increased the expression of *Il6* after nine days in culture with M(LPS) CM (Figure 1F). Additionally, we observed an increase in ECM deposition following treatment with an inflammatory medium (Figures 1G and 1H), strengthening the link between inflammation and ECM deposition. The increase in ECM deposition was not associated with a parallel rise in ECM-related gene expression (Figures S2B and S2C). Thus, the excessive ECM accumulation of collagen might also be regulated at the post-translational level.[39] We also exposed BAPs to hypoxic conditions. We performed a time course experiment where BAPs were cultured in either normoxic (21% O_2) or hypoxic (5% O_2) conditions. We validated our hypoxic model showing that *Glut1* expression was significantly higher in hypoxic than in normoxic conditions (Figure S2D). Compared with BAPs exposed to M(LPS) CM, "hypoxic" BAPs did not show higher expression of *Il6* than "normoxic" cells (Figure 1I). However, "hypoxic" BAPs did show significant increase in *col1a2* gene expression (Figure S2E). In addition, Collagen1 and FN deposition was higher in hypoxic conditions than normoxic ones (Figures 1J and 1K). These results indicated that BAT's hypoxic and inflammatory environment, as observed in response to HFD, activated the BAPs' profibrotic program.

Fibro-inflammation impairs brown adipocyte functions *in vitro*

BAPs exposed to M(LPS) CM showed lower expression of *Pparγ2* and the brown markers *Ucp1* and *Pgc1α*, as well as reduced lipid droplet accumulation compared with control conditions (Figures 2A–2D). We confirmed in the PAZ6 cell line that human brown preadipocytes respond similarly to macrophage stimulation. Thus, PAZ6 cells treated with M(LPS) CM showed reduced adipogenic capacity (i.e., lower lipid droplet accumulation and brown marker expression) and higher collagen and FN production (Figures S3F–S3H). Similarly, BAPs exposed to hypoxic conditions showed impaired differentiation capacity (Figures 2E and 2F). These results indicate that inflamed macrophages and hypoxia can activate BAPs toward a profibrotic profile and impair their brown adipogenic potential.

To dissect the specific role of BAT fibrosis on brown cell functionality, we used an 'in-house' developed three-dimensional (3D) culture system to uncouple fibrosis from macrophage-induced inflammation. We reproduced the BAT fibro-inflammatory environment using fibrotic fibers extracted from BAT of obese ($Lep^{ob/ob}$) or lean ($Lep^{wt/wt}$) mice as previously described.[16] Compared with wild-type (WT) mice, obese ($Lep^{ob/ob}$) mice showed a reorganization of the ECM network and higher gene expression of collagens (Figures S4A and S4B). Also, *Pepd* expression was reduced in BAT from obese mice compared with WT (Figure S4B). After tissue decellularization, the matrix fibers were imaged, showing more dense and aligned collagen fibers as a hallmark of fibrosis[40] (Figure S4C). We used a hydrogel in which BAPs were embedded and co-cultured with or without (3D control) matrix fibers isolated from BAT of obese ($Lep^{ob/ob}$) or lean ($Lep^{wt/wt}$) (Figure S4D). When cultured in ECM ($Lep^{WT/WT}$ and $Lep^{ob/ob}$), BAPs showed reduced lipid droplet accumulation and expression of brown markers during adipogenesis compared with the 3D control condition (Figures 2G–2K). As adipocytes were cultured with a similar quantity of ECM from "lean" or "obese mice," proportional to the level of fibrosis in BAT, we rationalized that the down-regulation of brown marker expression observed in the presence of ECM was primarily resulting from biomechanical effects of the collagens on the adipocytes as described previously.[16] However, when focusing on the effect of the "obese" ECM *versus* "lean" one, we showed that the addition of ECM from $Lep^{ob/ob}$ mice also lowered mRNA expression of brown adipocyte markers *Ucp1*, *Prdm16*, and *Pparγ* compared with BAPs cultured with ECM from lean $Lep^{WT/WT}$ mice (Figures 2H–2K). These results indicated that the anti-adipogenic effect of "obese" $Lep^{ob/ob}$ ECM was more severe than with "lean" ECM. However, the deleterious functional impact exacerbated by the "obese" ECM also suggested a biochemical effect of

Figure 2. Fibro-inflammation impairs brown adipocyte functions in vitro

(A–C) mRNA expression of adipogenic markers *Pgc1α* (A), *Ucp1* (B), and *Pparγ2* (C) during time course differentiation of C57BAT cells cultured without (control; n = 6) or with conditioned medium from LPS-stimulated BMDM (M[LPS] CM; n = 6).

(D–G) Representative images of confocal analysis of BODIPY (green) and actin (red) staining and corresponding quantifications of and lipid droplet accumulation in C57BAT (D) and pBAT (E and G) cells cultured with conditioned medium from M(LPS) CM (n = 6) compared with control (D; n = 6), cultured in hypoxia condition (5% O_2, n = 6) compared with normoxia (21% O_2, n = 6) (E), or cultured in 3D hydrogel with BAT of lean $Lep^{wt/wt}$ (n = 5) or obese $Lep^{ob/ob}$ mice (n = 5) after 6 days of differentiation. Scale bars: 50 μm (D and G) and 100 μm (E). (F) mRNA expression of brown markers in differentiated pBAT cells cultured at 21% O_2 (normoxia; n = 6) or 5% O_2 (hypoxia; n = 6).

(H–K) mRNA expression of *ucp1* (H), *prdm16* (I), *pgc1α* (J), and *pparγ2* (K) in pBAT differentiated adipocytes cultured in 3D hydrogel alone (3D; n = 4) or with BAT of either lean $Lep^{wt/wt}$ (n = 4) or obese $Lep^{ob/ob}$ mice (n = 4) and stimulated or not (control) with NE for 24 h.

(L) Fold change release of glycerol in 4 h NE-stimulated pBAT cultured in 3D hydrogel alone (3D; n = 4) or with BAT of either lean $Lep^{wt/wt}$ (n = 4) or obese $Lep^{ob/ob}$ mice (n = 4), compared with basal condition.

Data are presented as mean ± SEM. Two-way ANNOVA with Šidák's post hoc multiple-comparisons test was used to compare day 9 with day 0 in control and M(LPS) CM conditions (A–C) and to compare the ECM effect with control (H–K). Student's t test was used to compare control/M(LPS) CM conditions (D) and normoxia/hypoxia conditions (E and F). One-way ANOVA with Dunnett's post hoc multiple-comparisons test was used to compare the ECM effect with control (G and L).

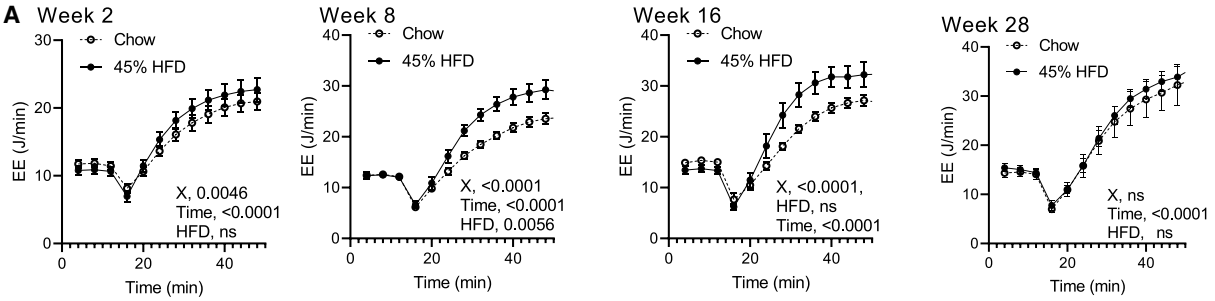

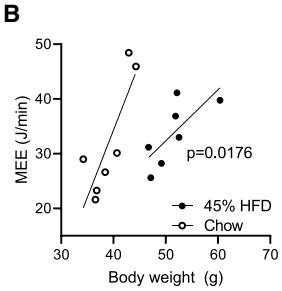

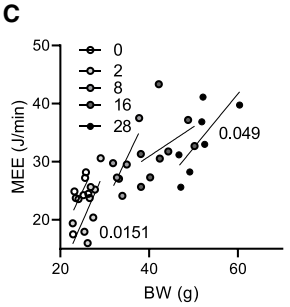

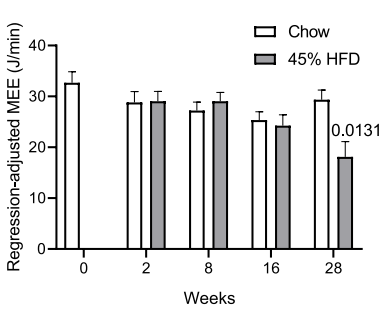

E

Model		B	SE B	β	t	p
4	(Intercept)	3.018	2.879		1.048	0.299
	BW	0.810	0.098	1.091	8.248	$1.469e^{-11}$
	Peri-AD coll	-0.912	0.376	-0.243		0.018
	Diet X weeks	-0.191	0.093	-0.275	-2.056	0.044

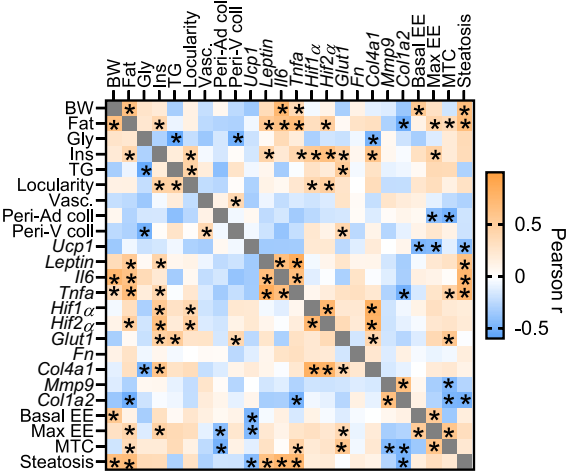

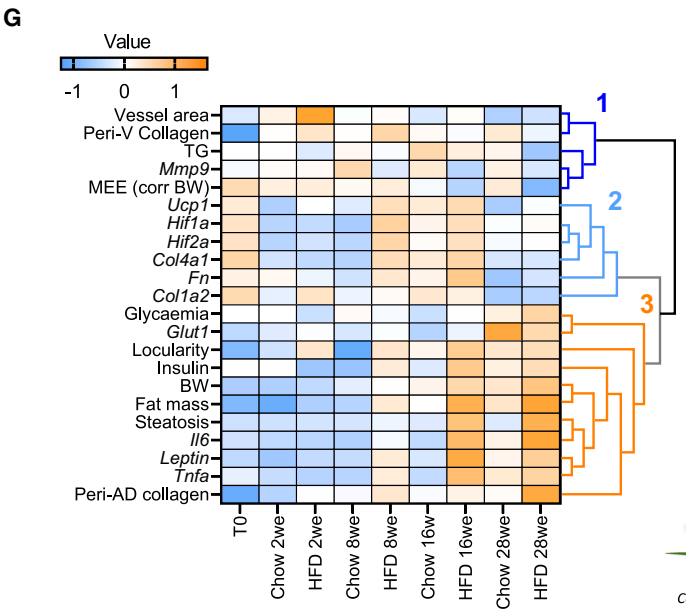

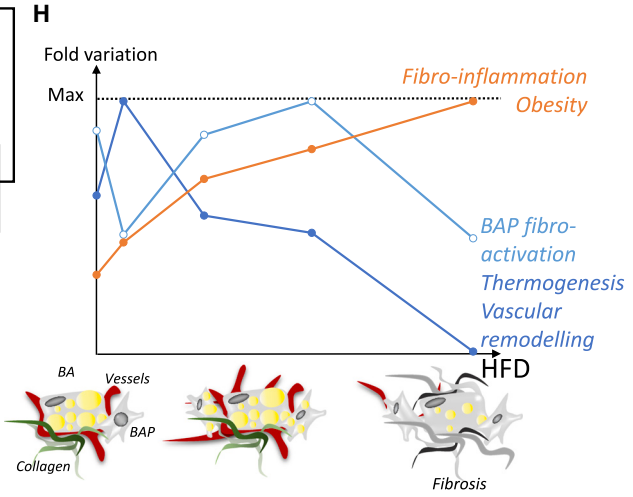

(legend on next page)

the "obese" ECM composition on adipocytes. We also tested thermogenic marker expression in response to norepinephrine (NE) stimulus. Ucp1 expression was induced after 24 h NE stimulation in our experimental condition. Of relevance, we found that the combination of "obese" *Lep*$^{ob/ob}$ ECM and NE downregulated brown markers (*Prdm16* and *Pgc1α*). Also, BAPs cultured in "obese" ECM (but not "lean") showed a reduced NE-induced glycerol release compared with 3D control BAPs (Figure 2L). Altogether, these experiments confirm a direct detrimental effect of BAT ECM extracted from obese mice on BAP differentiation and lipolysis activity.

BAT thermogenesis is impaired during a long-term HFD in association with the development of fibro-inflammation in BAT

Assessment of maximal thermogenic capacity (MTC), which refers to the highest amount of heat a mouse can produce, provides a direct measure of BAT function.[41] No studies have reported the long-term effects of HFD on established obesity beyond four weeks.[30] To investigate whether BAT fibro-inflammation prevents BAT activation *in vivo*, we assessed EE in response to NE at specific time points during the HFD. We measured the NE-stimulated EE of HFD-fed mice compared with chow-fed animals (Figures 3A and S5A). Mice on HFD showed increased BW and higher maximum respiration than control animals upon adrenergic agonist administration after 8 and 16 weeks of HFD (Figure 3A). Despite HFD-fed mice being larger than chow-fed animals at 28 weeks of HFD, there was no difference in the maximal EE achieved by both groups (Figure 3A). When corrected for BW using analysis of covariance (ANCOVA), the maximum NE-stimulated EE in 28 weeks of HFD-fed mice was lower than in respective controls, suggesting they had a disproportionately low NE-stimulated EE (Figures 3B and S5B). In addition, when BW was considered using covariance, we also observed that maximal EE was significantly reduced as a function of age in chow-fed and HFD-fed mice (Figures 3C, 3D, and S5B).

Although a substantive proportion of the EE in response to NE is expended in BAT, our data could not rule out changes in NE responsiveness occurring in other organs. We next performed multiple linear regression to determine if BAT fibrosis changes were associated with NE-stimulated heat production changes. We initially included BW, age, and diet as variables. Given the results of the ANCOVA analyses, we also included the diet × time interaction variable in our regression model. We conducted a stepwise regression model to determine the best predictors of EE in our dataset. Three valid models were generated (models 2, 3, and 4; model 1 considering no predictors): BW alone (model 2); BW and peri-AD collagen (model 3); and BW, peri-AD collagen, and the interaction of diet × weeks (model 4) (Figures 3E and S6). Age and diet were not included in any model, as their effects were captured by their impact on BW. The best model was model 4 (maximal EE; $F(3, 62) = 33.498$, $p = 5.388e^{-13}$, $R^2 = 0.618$) (Figure 3E). We found a significant relationship between maximal EE and BW (higher BW correlated with higher maximal EE; $\beta = 1.091$, $p = 1.469e^{-11}$), peri-AD collagen (higher BAT fibrosis correlated with lower maximal EE; $\beta = -0.243$, $p = 0.018$), and the interaction of diet × weeks (the longer the mice are on HFD, the lower is the maximal EE; $\beta = -0.275$, $p = 0.044$). Thus, these results indicated that BAT fibrosis, due to prolonged high-fat feeding, was a negative predictor of NE-stimulated EE, even when accounting for the positive relationship between BW and maximal EE. Our results indicate that the inclusion of BAT fibrosis and the interaction of HFD × length of the diet as covariates resulted in the highest proportion of variance explained in maximal EE (0.786) compared with other models (Figures 3E and S6A), indicating the significant role of BAT fibrosis and chronicity of the HFD in limiting maximal EE in obese mice.

We performed a correlation matrix and cluster analysis to elucidate the relationship between multiple metabolic parameters, fibro-inflammation, and dietary conditions. We first investigated the correlation between each parameter. In line with our initial results, we found that the HFD-induced BW gain was associated with BAT inflammatory markers (e.g., *Il6* and *Tnfα* expression) and liver steatosis (Figure 3F). Induction of hypoxic markers (e.g., *Hif1α*, *Hif2α*, *Glut1*) was associated with HFD-induced hyperinsulinemia and BAT whitening). Also, increased BAT collagen deposition was associated with reduced maximal EE, strengthening the link between obesity, BAT fibro-inflammation, and impaired thermogenic capacity.

Figure 3. BAT thermogenesis is impaired during a long-term high-fat diet (HFD) in association with the development of fibro-inflammation in BAT

(A) NE-stimulated EE, expressed as EE over time, in C57Bl/6 mice housed at 21°C and fed 2, 8, 16, or 28 weeks (n = 6/group) with chow diet or HFD 45%.

(B) Maximal NE-stimulated EE plotted against body weight (BW) from C57Bl/6 mice fed 28 weeks chow (n = 7) or HFD 45% (n = 7).

(C) Uncorrected maximal EE plotted against BW from C57Bl/6 mice fed 2, 8, 16, or 28 weeks with a chow diet.

(D) NE-stimulated EE (MEE) in C57Bl/6 mice housed fed 2, 8, 16, or 28 weeks with chow diet or HFD 45%, corrected for BW by ANCOVA covariates assessed at BW = 33.95 g ± SEM.

(E) Multiple regression analysis of the association between the maximal EE, BW, peri-adipocyte collagen in BAT (peri-AD coll), and the interaction between weeks and diet (diet × weeks). Unstandardized (B) and standardized (β) coefficients are presented as well as SE and t and p values.

(F) Pearson correlation matrix between BAT ECM remodeling markers and metabolic and thermogenic parameters in mice fed 2, 8, 16, or 28 weeks with HFD 45%.

(G) Heatmap showing clustering of metabolic, thermogenic, and BAT ECM remodeling parameters during chow and HFD 45%. Original values were ln(x + 1) transformed. Pareto scaling was applied to rows. Both rows and columns were clustered. Dendrograms indicate the tightness of clusters. Cluster 1, "EE, vascular remodeling"; cluster 2, "BAP fibro-activation"; cluster 3, "fibro-inflammation, obesity."

(H) Representation of the cluster analysis in (G) into a hypothetic scheme representing the 3 main clusters of metabolic, thermogenic, and BAT ECM remodeling parameters and their pattern of variation during the course of obesity: cluster 1, "EE, vascular remodeling"; cluster 2, "BAP fibro-activation"; cluster 3, "fibro-inflammation, obesity." Max, maximal level of regulation.

Data are presented as mean ± SEM. Two-way ANOVA with Šidák's post hoc multiple-comparisons test was used to compare the HFD effect during the time course (A).

Next, we performed cluster analysis, placing mice into three main clusters according to diet and time point (Figure 3G). The parameters investigated were grouped into three clusters. The first cluster was "thermogenesis and vascular remodeling" and included vascularization and EE-related parameters. These parameters were upregulated in the early stage of HFD and then strongly decreased during the long-term HFD. A second cluster, labeled "BAP fibro-activation," defined by BAP markers (Ucp1 and ECM components), was initially downregulated and followed by substantial up-regulation at 16 weeks of HFD. Finally, the third cluster, "fibro-inflammation and obesity," including fibrosis deposition, mRNA expression of inflammatory markers, metabolic parameters, and BW, was gradually upregulated during whole time course HFD. These analyses suggested a two-phase activation of BAPs upon HFD: (1) initial recruitment to promote thermogenesis in association with vascular remodeling and (2) activation in the chronic phase of obesity in response to inflammatory stimuli, leading to ECM deposition. Interestingly, EE and vascular remodeling were rapidly impaired in response to positive energy balance and associated fibro-inflammation, reinforcing the role of unbalanced ECM remodeling and subsequent fibro-inflammation in promoting BAT dysfunction during the development of HFD-induced obesity (scheme in Figure 3H).

Partial *Pepd* ablation exacerbates obesity-induced fibro-inflammation in BAT

We then investigated the relevance of ECM remodeling in BAT in response to HFD. As a model for impaired ECM remodeling, we used *Pepd*-heterozygous (HET) mice, which spontaneously develop fibro-inflammation in WAT associated with adipose dysfunction (e.g., blunted response to NE and impaired adipogenesis).[37] We used a chronic model of obesity where mice were fed HFD 58% for 28 weeks, known to induce severe WAT fibro-inflammation associated with chronic obesity.[37] We validated that WT mice fed HFD showed significantly increased expression of *Ucp1* (only at 12 weeks of HFD) and higher EE, as previously reported in DIO models (Figures 4A–4C). WT HFD-fed mice showed lower *Pepd* expression, higher expression of ECM (both fibrillar and non-fibrillar collagens), inflammatory markers, and higher collagen deposition in BAT than chow-fed mice (Figures 4A, 4B, 4D, and 4E). In addition, a higher level of BAT fibrosis was associated with higher BW, insulin resistance (homeostatic model assessment for insulin resistance [HOMA-IR] index), BAT whitening, and a higher level of fibro-inflammatory marker gene expression (Figure 4G). As observed in WAT,[37] the *Pepd*-HET mice showed higher collagen deposition around brown adipocytes (peri-AD collagen) in chow-fed conditions (Figures 4D and 4E). Interestingly, collagen content was similar among genotypes in HFD condition despite a tendency for higher gene expression levels of collagens in BAT from HET mice compared with WTs (Figures 4D, 4E, and 4H). We rationalized that because prolonged obesity in the WT mice down-regulates *Pepd* expression, impaired collagen turnover differences are attenuated between *Pepd*-HET and WT mice fed HFD. However, we did observe differences in metabolic changes. Metabolic complications of obesity (i.e., liver steatosis, insulin resistance, and lipolysis) were exacerbated in *Pepd*-HET mice fed 58% HFD as previously reported in the present mice cohort.[37] This study shows that *Pepd*-HET mice displayed bigger lipid droplets in BAT when fed HFD than WT mice (Figure 4F). Partial *Pepd* ablation also led to reduced *Ucp1* and *Pparγ2* expression compared with WTs (Figure 4H), lower *Pepd* expression associated with insulin resistance (HOMA-IR index), higher *Col1a2* expression, and the association between ECM components and inflammatory markers was greater in HET mice compared with WTs (Figure 4I). Taken together, we showed that unbalanced ECM remodeling in BAT leads to fibro-inflammation, ultimately limiting BAT activation capability. Correlation studies also suggested a potential role of inflammation in promoting BAT fibrosis and subsequent dysfunctions that are exacerbated in obese HET mice.

Given that inflammation and fibrosis are related events, we investigated the contribution of macrophages in promoting fibrosis and BAT dysfunctions in the *pepd*-HET model. We conducted a bone marrow transplantation (BMT), transferring myeloid cells from *Pepd*-depleted mice to WT mice (BMT mice) as previously described.[37] Although *pepd*-HET mice displayed exacerbation of BAT fibro-inflammation, it was not worsened in BMT knockout (KO) mice compared with WT mice. BMT KO mice showed a slight increase in fibrosis levels compared with WT mice under chow-fed conditions but similar ECM gene expression (Figure S5C). Furthermore, HFD-fed BMT KO mice had reduced whitening of BAT and similar expression of *Ucp1* and *Pparγ2* compared with WT mice (Figures S5E and S5F). These results indicate that while macrophages have a significant role in fibrosis deposition, other factors or cell types contribute to exacerbating BAT dysfunctions in *Pepd*-HET mice.

Fibro-inflammation is a hallmark of inactive BAT in humans

We then investigated the relevance of ECM remodeling and fibro-inflammation on BAT activation in human subjects. We reanalyzed our RNA-seq dataset performed on BAT biopsies obtained from the supraclavicular region in cold-exposed subjects (GEO: GSE113764[42]) and assessed if and how genes related to ECM remodeling correlated with BAT activity and clinical parameters. Interestingly, we found that high expression of collagen (notably collagen 1, 3, 5, and 6), some MMPs (e.g., *MMP2*), and profibrotic factors (i.e., *INHBB* and *INHBA*) was associated with lower expression of *UCP1* and/or low cold-stimulated BAT activity (i.e., glucose uptake) and a higher level of cholesterol in the blood (Figures 5A–5C). In addition, we found that when the cold-exposed subjects were categorized into high-BAT and low-BAT groups on the basis of cold-stimulated BAT glucose or fatty acids uptake (high BAT, glucose uptake $\geq$ 3.0 μmol/100 g/min or nonesterified fatty acid (NEFA) uptake $\geq$ 0.7 μmol/100 g/min), significantly higher expression of collagen was observed in low-BAT subjects compared with high-BAT subjects. This result suggests fibro-inflammation as a hallmark of less active BAT in humans (Figure 5D). A similar conclusion was obtained when individuals were grouped according to BAT *UCP1* expression, with higher expression being associated with down-regulation of fibro-inflammatory pathways (i.e., "ECM organization," "NF-κB signaling," and "TGF-β signaling") (Figure S7A). Together, these results align with our mice study, supporting a link among BAT ECM remodeling, fibro-inflammation, and impaired BAT activation.

CellPress
OPEN ACCESS

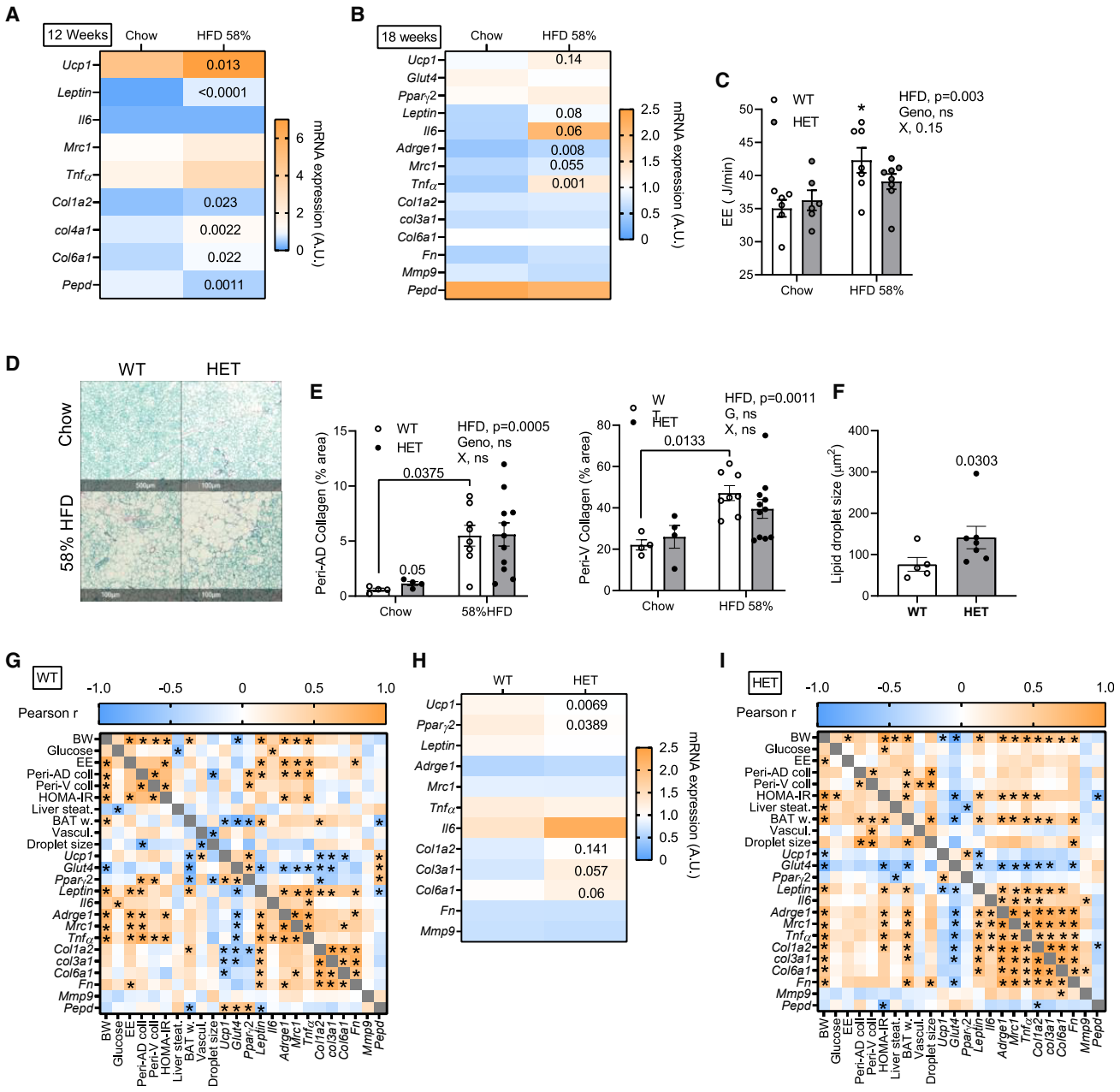

Figure 4. Down-regulation of *Pepd* exacerbates BAT fibro-inflammation in DIO mice

(A and B) Heatmaps of mRNA expression of brown and fibro-inflammatory markers in BAT from C57bl/6 mice fed 12 weeks (A; n = 8) or 18 weeks (B; n = 8) with HFD 58% compared with chow-fed mice (n = 8/6, respectively).

(C) Forty-eight hour energy expenditure in *Pepd* WT and HET mice fed chow (n = 6/group) or 58% HFD (18 weeks, n = 7/group).

(D and E) Representative images of red Sirius staining in BAT from *Pepd* WT and HET mice fed chow (n = 4/group) or 58% HFD (18 weeks, n = 8/10, respectively) (D) and corresponding quantification of peri-adipocyte (peri-AD) and peri-vascular (peri-V) collagen deposition represented as percentage tissue area (E). Scale bar: 100 μm.

(F) Lipid droplet area in BAT from *Pepd* WT (n = 5) and HET mice (n = 6) fed 58% HFD (18 weeks).

(G–I) Pearson correlation matrix between BAT ECM remodeling markers and metabolic and thermogenic parameters in *Pepd* WT (G) and HET mice (I) fed chow (n = 4/group) and 58% HFD (18 weeks, n = 8/10, respectively). (H) Heatmaps of mRNA expression of brown and fibro-inflammatory markers in BAT from *Pepd* WT (n = 8) and HET mice (n = 10) fed 58% HFD (18 weeks).

Data are presented as mean ± SEM. Two-way ANNOVA with Tukey's post hoc multiple-comparisons test was used to compare WT and HET mice (C, E, and F). Student's *t* test was used to compare chow- and HFD-fed mice (A and B) and WT and HET mice (F and H).

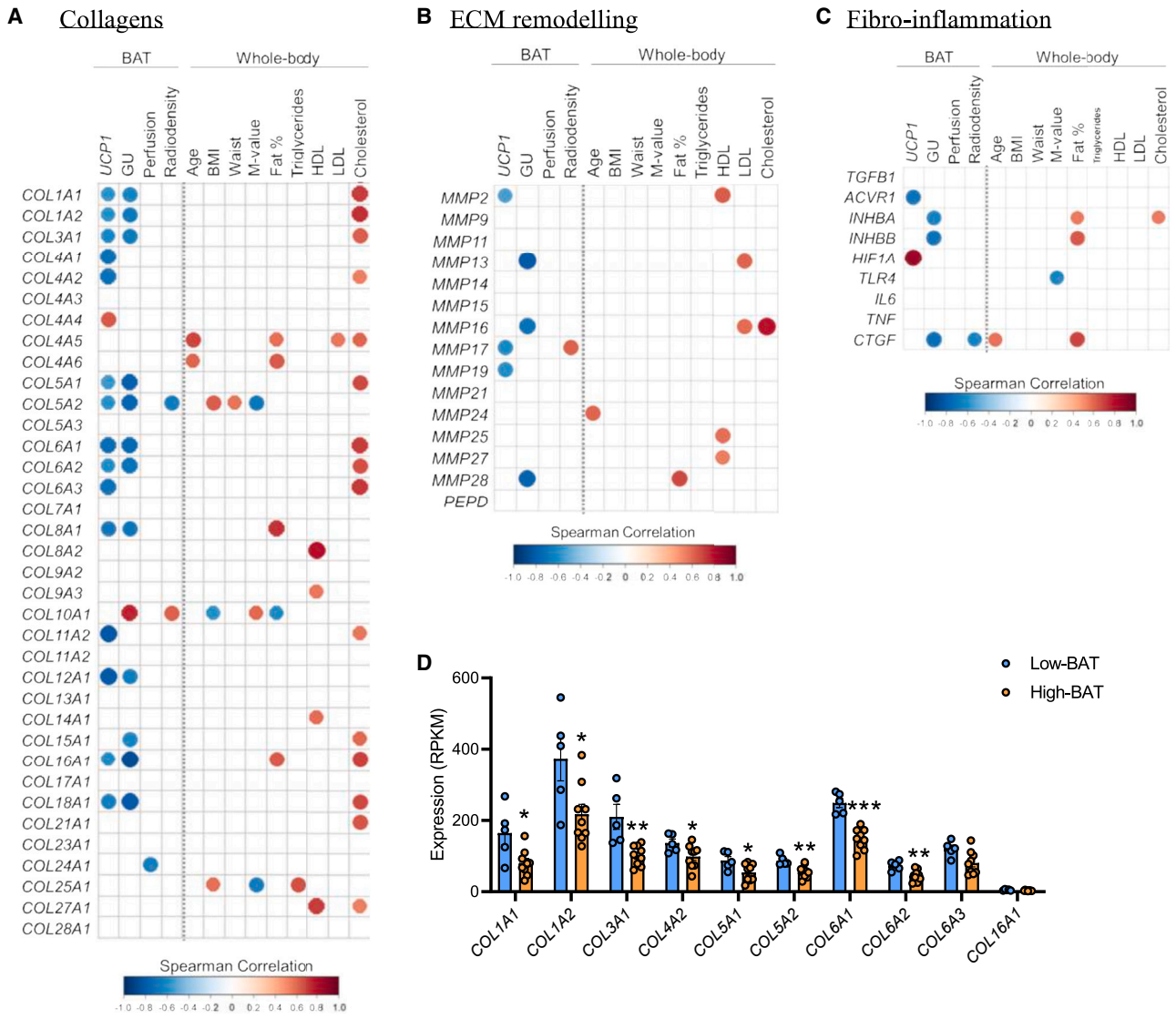

Figure 5. Fibro-inflammation is a hallmark of inactive BAT in humans

(A–C) Spearman correlation between expression of collagens (A), ECM remodeling-related markers (B), fibro-inflammatory markers (C), and BAT activation markers and whole-body systemic metabolic parameters.

(D) Comparison of expression of collagens in BAT between the subjects exhibiting high- or low-cold-stimulated BAT metabolic activity. *p < 0.05 compared with low-BAT using t test.

Activation of human and murine brown adipocytes is associated with ECM remodeling

We then examined how ECM was regulated during brown adipocyte activation and recruitment in humans and mice at the cellular level. We observed that brown adipogenesis was associated with changes in collagen expression characterized by increased basement membrane components *col4a1* and *col6a1* in primary murine brown adipocytes (Figure S7B). In line with these results, we found that differentiation of the human brown adipocyte cell line (PAZ6,[43] GEO: GSE168387) was associated with down-regulation of fibro-inflammatory pathways (i.e., wound healing and TNF signaling pathway), including fibrillar collagen and cross-linking regulatory proteins (e.g., *COL1A2*, *LOX*, SPARC) (Figures 6A and 6B). Of note, brown adipogenesis also involves up-regulation of ECM components, such as collagen 4 and 6, and laminin, typically associated with basement membrane formation characteristic of mature adipocyte ECM[44] (Figure 6B). These results indicate that ECM remodeling is correlated with brown adipogenesis. As observed in white adipose cells, brown adipogenesis replaces fibrillary collagen (e.g., collagen 1 and 3) with non-fibrillar collagen and basement membrane components (e.g., collagen 4).[45]

To assess the regulation of ECM remodeling in brown cell activation, we reanalyzed an RNA-seq dataset of human differentiated brown adipocytes isolated from supraclavicular AT of non-diabetic participants and stimulated for 4 h with NE

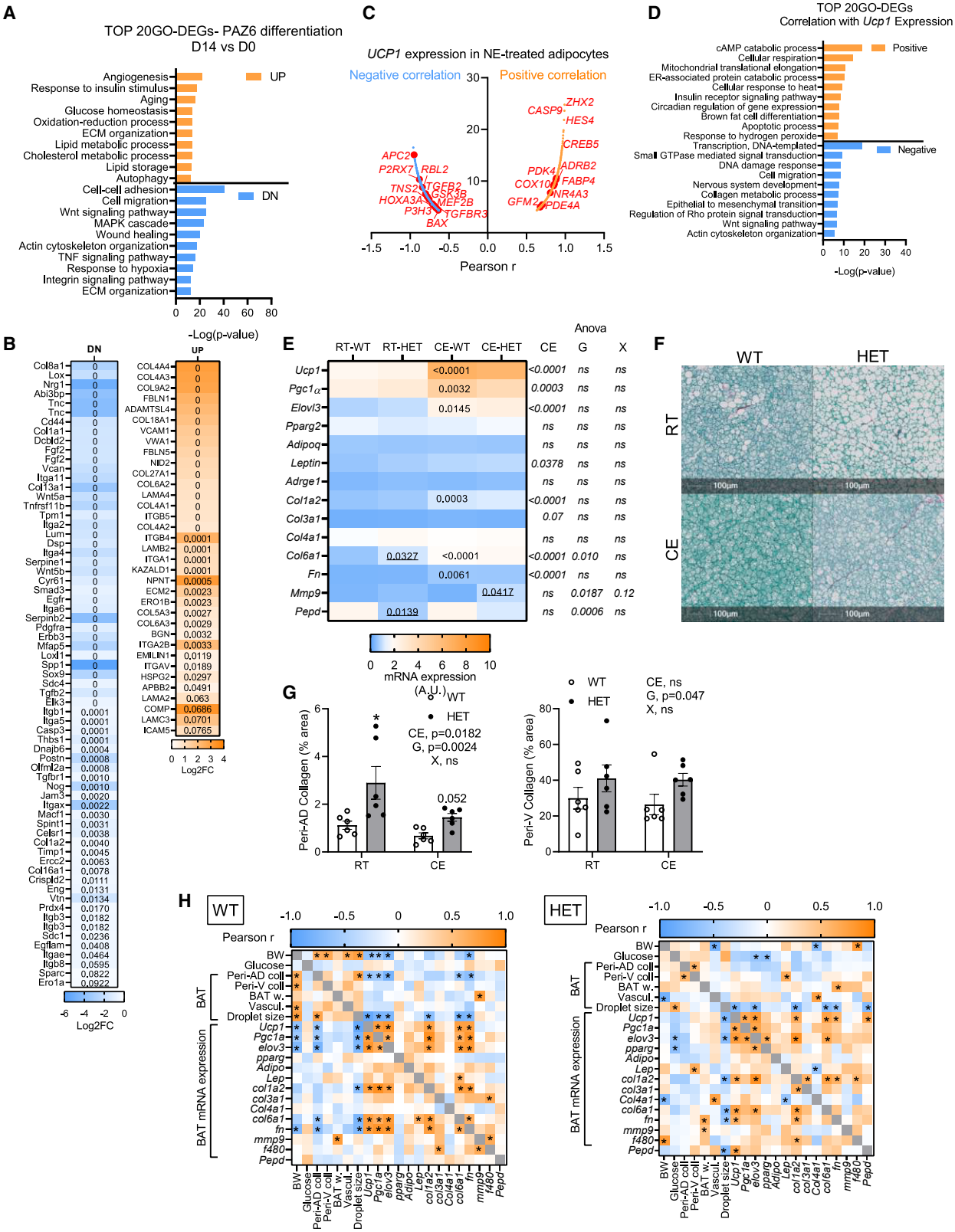

(legend on next page)

(10 μM).[46] We identified genes and pathways associated with *UCP1* expression in BAT (Figures 6C and 6D). As expected, the genes positively associated with *UCP1* were involved in human brown fat differentiation (e.g., *ADRB2*, *FABP4*) and cell respiration (e.g., *COX10*, *NR4A3*). In contrast, high *UCP1* expression was associated with down-regulation of collagen metabolic processes (e.g., *P2RX7*, *P3H3*) and epithelial-to-mesenchymal transition (e.g., *TGFB2*, *TGFBR3*), both pathways related to fibrosis.[8] In line with these human data, we found that pharmacological activation of differentiated primary murine brown adipocytes *in vitro* through adrenergic stimulation (NE) reduced collagen gene expression (Figure S7C). As observed during adipogenesis, these results indicate that brown adipocyte activation is associated with ECM remodeling and down-regulation of fibro-inflammation.

Cold-induced BAT activation is associated with ECM remodeling

We then studied the relevance of ECM remodeling in BAT activation following cold exposure (CE). As observed in the DIO model, the *Pepd*-HET mice showed higher collagen deposition around brown adipocytes (peri-AD collagen) both at room temperature (RT) and CE compared with WT mice (Figures 6F and 6G). Among the main ECM-related components of the BAT, only *Col6a1* mRNA expression was higher in *Pepd*-HET mice than WTs at RT (Figure 6E). Interestingly, *Pepd*-HET mice did not show variation in macrophage marker *Adrge1* in BAT at both RT and CE (Figure 6E).

We confirmed that BAT from WT mice acclimated to cold (3 weeks) showed increased expression of brown markers (*Ucp1*, *Pgc1α*, *Elovl3*) and reduced lipid droplet size compared with mice at RT (Figures 6E, S6A, and S6B). However, *Pepd*-HET mice did not show significant differences in lipid droplet size or brown marker gene expression compared with WTs at RT and upon CE (Figures 6E, S8A, and S8B). BW and blood glucose levels were not different between CE and genotypes (Figures S6C and S6D). Regarding the ECM profile, mRNA expression of ECM components (*Col1a2*, *Col6a1*, and *Fn*) in BAT increased following CE compared with RT in WT and HET mice (Figure 6E). However, the amount of collagen in BAT from CE mice was lower than at RT (in both WTs and HETs). It did not correlate with the increased gene expression observed (Figures 6F–6H), suggesting increased collagen turnover during CE. A correlation matrix analysis confirmed the expected association between BAT activation following CE (i.e., mRNA expression of brown markers) and low BW (Figure 6H). Also, the gene expression of fibrosis-associated ECM components (i.e., *Col1a2*, *Col6a1*, and *Fn*) correlated positively with the increase of brown adipocyte markers, including *Ucp1*, *Pgc1α*, and *Elovl3* in WT, and to a lesser extent in HET mice. However, peri-AD collagen content in BAT was associated with higher BW, bigger lipid droplets and lower brown marker gene expression in WT but not in HET mice (Figure 6H). These results indicated a link between collagen deposition and impaired BAT activation, which was less evident in the less cold-responsive HET mice. In line with a reduced response to cold, correlation matrix analysis in HET mice revealed that lower *Pepd* expression was associated with bigger lipid droplets and lower *Ucp1* expression (Figure 6H). However, without inflammation, the imbalance in collagen turnover did not significantly impair BAT activation upon CE.

BAT inactivation is associated with unbalanced ECM remodeling and fibro-inflammation

To further characterize ECM remodeling during the process of BAT activation, we re-analyzed the RNA-seq dataset from Sanchez-Gurmaches et al.[47] (GEO: GSE96681). In this study, mice were acclimated to cold for 3 weeks or acclimated for 3 weeks at 30°C (TN), an environmental temperature at which BAT stimulation by the sympathetic nervous system (SNS) is inactivated. Comparison between these opposite BAT activation states showed a strong up-regulation of the inflammatory response pathway in TN vs. CE (Figure 7A). From the repertoire of inflammatory markers, gene expression of cytokines and chemokines related to macrophage recruitment, such as *Cx3cl1*, *Ccr2*, and *Cxcl9*, was significantly increased in TN compared with CE. In addition, TN mice showed up-regulation of ECM organization genes, particularly fibrillary and fibrotic components such as collagens 1, 3, and 6 and MMPs (Figures 7B and 7C). Interestingly, *Pepd* was downregulated in TN compared with CE mice (Figure 7C). This dataset again indicates that inactive BAT is associated with fibro-inflammation and down-regulation of the prolidase PEPD.

We then investigated the effect of TN on BAT function and ECM profile in *Pepd* WT and HET mice. We confirmed that WT mice exposed to TN displayed reduced brown marker gene expression, increased inflammatory marker *Tnfα* and BAT whitening (i.e., bigger lipid droplets) (Figures S8E–S8G). We validated that *Pepd* gene expression was also significantly lower at TN than RT in WT mice (Figure S8E). Also, *Pepd* expression was negatively correlated with the size of lipid droplets

Figure 6. BAT activation is associated with ECM remodeling

(A and B) Gene Ontology (GO) enrichment analysis of differentially expressed genes (DEGs) in PAZ6-differentiated adipocytes compared with non-differentiated cells (A) and heatmaps of the DEGs related to the "ECM composition" pathways (B).

(C and D) *UCP1*-genes correlations in NE-stimulated differentiated adipocytes isolated from Tran et al. cohort,[46] shown as volcano plots (C) and GO enrichment analysis of the corresponding genes (D).

(E) Heatmaps of mRNA expression of brown and fibro-inflammatory markers in BAT from *Pepd* WT (n = 6) and HET (n = 6) mice housed at 21°C (RT) or acclimated to 8°C (CE).

(F and G) Representative images of red Sirius staining in BAT from *Pepd* WT (n = 6) and HET (n = 6) mice housed at 21°C (RT) or acclimated to 8°C (CE) (F) and corresponding quantification of peri-adipocyte (peri-AD) and peri-vascular (peri-V) collagen deposition represented as percentage tissue area (G). Scale bar: 100 μm.

(H) Pearson correlation matrix between BAT ECM remodeling markers and metabolic and thermogenic parameters in *Pepd* WT (n = 6) and HET (n = 6) mice housed at 21°C (RT) and acclimated to 8°C (CE).

Data are presented as mean ± SEM. Two-way ANNOVA with Tukey's post hoc multiple-comparisons test was used to compare WT and HET mice.

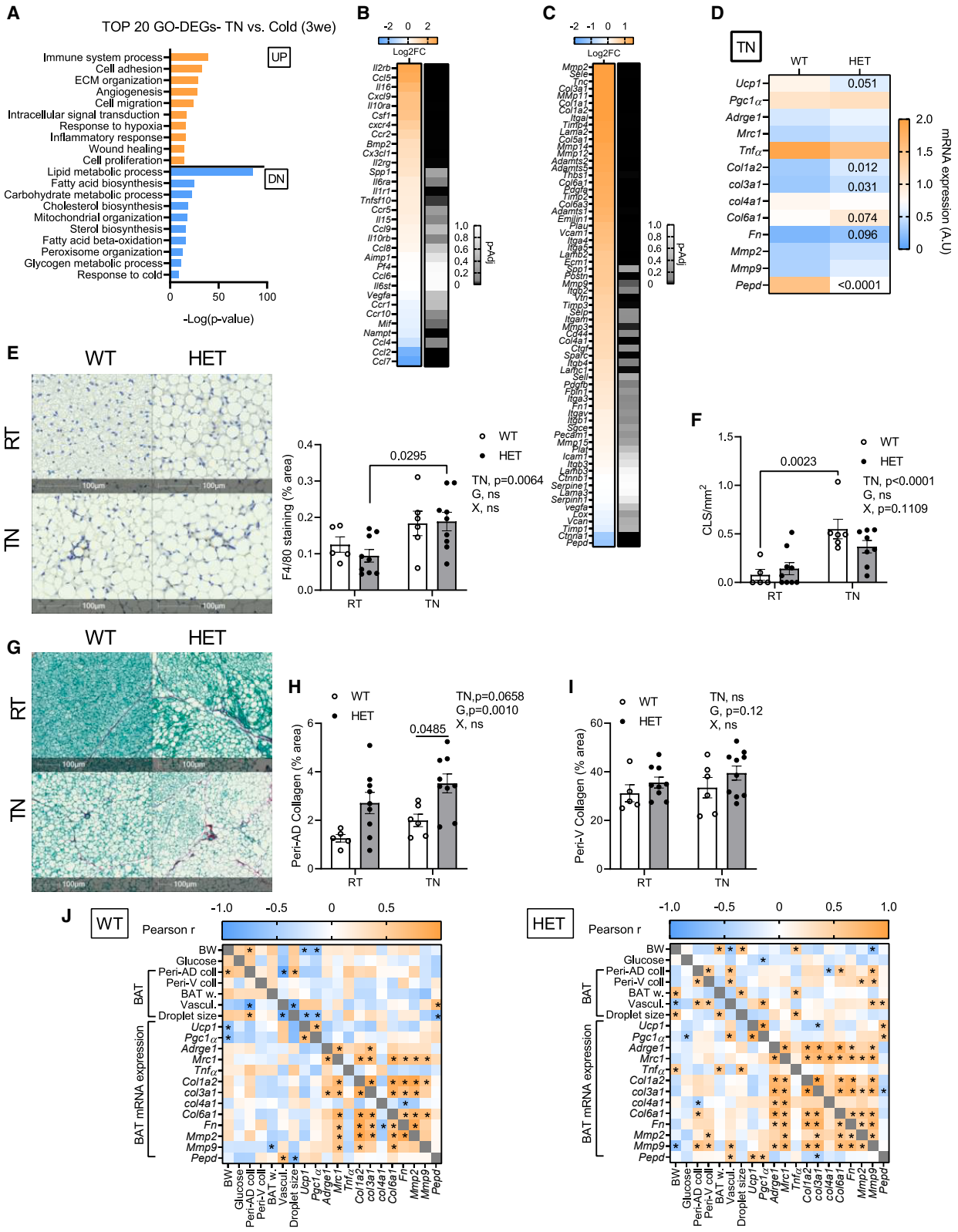

(legend on next page)

(Figure 7J). In line with the transcriptomic data, TN increases peri-AD collagen, macrophage accumulation (F4/80 staining) and crown-like structures (CLSs) compared with mice at RT, thus confirming the occurrence of fibro-inflammation at TN (Figures 7E–7I). In WT mice, peri-AD collagen deposition was associated with the whitening of the BAT. Higher collagen expression correlated with a higher level of *Mrc1* gene expression, a marker of macrophages involved in tissue remodeling[48] (Figure 7J).

As expected, *Pepd*-HET mice displayed higher peri-AD collagen deposition at RT and TN than their WT littermates (Figures 7G–7I). Still, they did not show a difference in the perivascular collagen. In addition, partial depletion of *Pepd* increased gene expression of fibrillar collagens 1 and 3 (but not basement membrane collagen 4 gene expression) (Figure 7D), suggesting exacerbated fibrosis. Interestingly, fibro-inflammation in BAT of HET mice was accompanied by decreased *Ucp1* gene expression compared with WTs (Figure 7D). In line with this, correlation matrix analysis showed that in HETs at TN, there was a more significant association between macrophage markers and fibrillar collagen gene expression, and lower *Pepd* expression was associated with lower *Ucp1* and *Pgc1α* gene expression (Figure 7J). Taken together, these results supported our human data showing fibro-inflammation as a hallmark of inactivated BAT.

DISCUSSION

Individuals with obesity have a decreased amount of responsive BAT; however, the cause-effect relationship between decreased BAT and obesity is unclear. Here we showed that obesity is associated with fibro-inflammation and impairment in its development and functionality. In humans, a fibro-inflammatory environment limits BAT activation. From this observation, we showed that BAT's recruitment, maintenance, and functionality requires tightly regulated ECM remodeling adjusted to environmental cues such as cold and HFD. We also showed that primary defects in ECM remodeling are sufficient to disrupt BAT recruitment and function.

Our human data suggest that dysregulation of ECM components in BAT may contribute to dysfunctional metabolism, as indicated by the inverse correlation between collagen expression and cold-induced BAT glucose uptake and *UCP-1* expression. We also observed a positive correlation between many collagens and plasma cholesterol levels, which may indicate a potential role for ECM dysregulation in lipid metabolism. However, further research is needed to confirm these associations in larger cohorts, particularly in obese individuals where fibro-inflammation may be more pronounced.

Upon cold stimulation, BAT undergoes active ECM remodeling, leading to reduced collagen levels and higher brown marker expression. Brown preadipocytes are the primary cells producing ECM, and downregulate ECM and inflammatory markers during adipogenesis and acute activation. These results align with recent findings showing a decreased expression of *Col1a1* in AMPc-treated adipocytes associated with increased protein release.[17] Inflammation is associated with impaired BAT function, and several anti-inflammatory molecules are upregulated upon BAT activation.[49,50] We compared the molecular characterization of BAT in TN versus CE and observed a down-regulation of inflammation in CE (activated) vs. TN (inactivated) BAT. Inactive BAT is associated with the enrichment of fibro-inflammatory pathways, as previously suggested by our human data. We confirmed the presence of fibro-inflammation in mice acclimated to TN, showing that BAT whitening was associated with a higher level of CLS and collagen deposition around adipocytes. BAT from mice with chronic obesity also shared features of fibro-inflammation. Therefore, we concur with Keijer et al.[51] that 30°C may not be the most suitable housing temperature for mice in preclinical studies, as it could mask the impact of obesity by promoting BAT fibro-inflammation and dysfunction even in chow lean supposed to be healthy mice.

The HFD time course study revealed that following an initial activation phase, BAT experienced progressive inactivation characterized by whitening, hypoxia, and fibro-inflammatory response during HFD, consistent with WAT observations[52] We observed higher collagen accumulation around adipocytes after 28 weeks of HFD compared with chow, coinciding with significantly higher Il6 expression. The occurrence of inflammation and fibrosis after 28 weeks of HFD suggests a failure of the BAT tissue in the context of sustained metabolic insult, ultimately leading to a pathological fibro-inflammation phenotype. These findings suggest that BAT fibrosis occurs similarly to WAT, as observed in later stages of obesity.[53] We also noticed a correlation between down-regulation of "vascular remodeling and thermogenesis" cluster and up-regulation of "BAP fibro-inflammation" cluster. This may indicate that BAT vessels rarefaction, local hypoxia, and activation of BAPs into profibrotic progenitors compromise BAT thermogenesis.

In WAT, the amount of AT fibrosis correlates with the number of AT macrophages (ATMs),[54] suggesting potential crosstalk between macrophages and preadipocytes mediating

Figure 7. BAT inactivation is associated with unbalanced ECM remodeling and fibro-inflammation

(A) GO enrichment analysis of DEGs in BAT from C57Bl/6 acclimated 3 weeks to 5C compared with mice acclimated 3 weeks to thermoneutrality (TN) (n = 4).[47]

(B and C) Heatmaps of inflammatory (B) and ECM-related DEGs (C) in BAT of mice acclimated 3 weeks to cold compared with mice housed at TN (n = 4) expressed as $\log_2$ fold change ($\log_2$FC) variation over TN.

(D) Heatmaps of mRNA expression of brown and fibro-inflammatory markers in BAT from *Pepd* WT and HET mice housed at 21°C (RT) or acclimated to 30°C (TN).

(E–I) Representative images of F4/80 (E) or red Sirius (G) staining in BAT from *Pepd* WT and HET mice housed at 21°C (RT; n = 5/9, respectively) or acclimated to 30°C (TN; n = 6/8, respectively) and corresponding quantification of F4/80 staining (E), crown-like structure (CLS) number expressed as percentage area (F), peri-adipocyte (peri-AD; H) and peri-vascular (peri-V; I) collagen deposition represented as percentage tissue area. Scale bar: 100 μm.

(J) Pearson correlation matrix between BAT ECM remodeling markers and metabolic and thermogenic parameters in *Pepd* WT and HET mice housed at 21°C (RT; n = 5/9 respectively) or acclimated to 30°C (TN; n = 6/8, respectively).

Data are presented as mean ± SEM. Two-way ANNOVA with Tukey's post hoc multiple-comparisons test was used to compare WT and HET mice (E, F, H, I). Student's t test was used to compare WT and HET mice (D).

fibro-inflammation.[55,56] Our *in vitro* data suggested that inflammatory macrophages induced ECM deposition in BAPs and prevented adipogenesis. Interestingly, similar results were observed in the condition of hypoxia. In addition, an obese ECM was detrimental to BAP differentiation and function. Further investigations are required to validate the impaired capacity of BAPs to differentiate and if any switch to fibrotic phenotype is observed *in vivo* in chronic obesity as observed in WAT.[57]

This study is the first to describe the gradual decline in MTC and BAT thermogenesis in response to HFD in mice. As Gransoch M et al. previously performed, we plotted individual data related to BW and analyzed the effects of HFD on MTC using covariance (ANCOVA).[20] We found that MTC was reduced in mice fed HFD for 28 weeks compared with chow-fed controls. Using a regression-based approach, Schwartz and colleagues showed that $Lep^{ob/ob}$ mice exhibit a significant reduction of EE relative to WT controls. However, the EE/lean body mass ratio comparison did not support this effect.[58] These results align with the thermogenic defects (i.e., decreased maximal calorigenic response and sensitivity to NE, decreased respiratory response to dibutyryl cyclic AMP (DcAMP), and decreased BAT cytochrome oxidase activity) observed in BAT of obese diabetic SHR/N-cp rats.[59] In our model of diet-induced obesity, we found that the collagen deposition in BAT was negatively correlated with thermogenic function once BW and time on diet were controlled for, which suggests that anti-fibrotic strategies could be a potential approach to maintain BAT functionality independently of obesity. Ablation of collagen-VI in obese $Lep^{ob/ob}$ mice improved metabolic phenotype by improving WAT, plasticity, and inflammation.[60] However, BAT was not investigated. More recently, Hasegawa et al. showed that repression of BAT fibrosis in *Gtf2ird1* transgenic mice improved systemic glucose homeostasis.[61] Further investigations are needed to decipher if removing fibro-inflammation in BAT could rescue BAT remodeling and activity in obesity.

We investigated the role of ECM remodeling in BAT fibro-inflammation using Pepd-heterozygote mice, which have 50% decreased expression of the prolidase PEPD, a key protein in collagen degradation and turnover.[12] We observed that the phenotype of *pepd*-HET mice differs among the different temperature/diet conditions. *Pepd*-HET mice showed a higher level of collagen deposition due to impaired collagen degradation independently from the diet/temperature condition. Of note, in the condition of HFD, WT mice also developed fibrosis which masked the differences with the HET mice, as observed in WAT.[37] *Pepd*-HET mice showed a mild phenotype when exposed to cold. When exposed to TN, *Pepd*-HET mice tended to have higher inflammation and lower expression of brown markers. However, *Pepd* depletion exacerbated BAT whitening and reduced the expression of brown markers in chronic HFD. The main difference among the groups that can explain the more robust phenotype in HFD-fed animals is the presence of inflammation. Both TN and HFD promote BAT inflammation. Interestingly, both conditions are associated with reduced expression of *pepd*. Our results suggest that further Pepd depletion exacerbates BAT dysfunction in these conditions. Further investigations are needed to determine and compare ECM composition at the protein level and changes in the organization of collagen fibers among cold, TN, and obesity conditions. Notably, decreased *Pepd* expression was a hallmark of fibro-inflammatory and inactive BAT observed at TN and chronic obesity. This evidence reinforced the importance of optimal collagen degradation and enhanced ECM remodeling to maintain BAT function and integrity.

Our study shows that appropriate ECM remodeling is critical for BAT function in response to physiological stimuli, and that failure of remodeling with inflammation leads to BAT dysfunction and atrophy. These findings suggest that therapeutics aimed at sustaining ECM remodeling and preventing fibro-inflammation could improve BAT maintenance and responsiveness, and potentially alleviate metabolic dysfunction in obesity.

Limitations of the study

We acknowledge that there are several limitations that must be considered. First, although we observed increased collagen expression in adipocytes in the context of obesity, further confirmation of the underlying mechanisms involved is required through single-nucleus/cell RNA-seq. Second, we showed that hypoxia is induced in BAT in response to HFD *in vivo*, and inhibits BAT adipogenesis and promotes ECM production *in vitro*. Additional research is necessary to validate the relationship between hypoxia and BAT fibro-inflammation and dysfunction, and to explore the associated mechanisms in mice and human. Third, the use of a heterozygote model with mild phenotypic responses in our study, suggests that an adipocyte-specific KO would be necessary to confirm the role of PEPD in regulating BAT ECM remodeling and BAT functions. Finally, our findings regarding the association between BAT activity and ECM expression were made in healthy lean subjects only, highlighting the need for further studies in larger cohorts of lean and obese individuals with different metabolic conditions to validate the link between BAT fibrosis, BAT activity, and metabolic complications.

STAR★METHODS

Detailed methods are provided in the online version of this paper and include the following:

- KEY RESOURCES TABLE
- RESOURCE AVAILABILITY
  - Lead contact
  - Materials availability
  - Data and code availability
- EXPERIMENTAL MODEL AND STUDY PARTICIPANT DETAILS
  - Animal models
  - Human subjects
  - Cell culture
- METHOD DETAILS
  - Magnetic-activated cell sorting
  - ECM preparation from decellularised BAT
  - Histological analysis
  - Immunofluorescence analysis and confocal microscopy
  - RNA extraction and real-time PCR
  - Lipolysis assay

- Calculation of energy expenditure and maximum thermogenic capacity
- QUANTIFICATION AND STATISTICAL ANALYSIS

SUPPLEMENTAL INFORMATION

Supplemental information can be found online at https://doi.org/10.1016/j.celrep.2023.112640.

ACKNOWLEDGMENTS

This work is supported by the Wellcome strategic award (100574/Z/12/Z); MRC MDU: MC_UU_12012/2 and MC_UU_12012/5 (The Disease Model Core, Biochemistry Assay Lab, Histology Core, and the Genomics and Transcriptomics Core); the Wellcome grant 10953/Z/15/Z (I.S.); the Wellcome Cambridge Trust scholarship (E.F.-J.); the Spanish Ministry of Economy and Competitiveness (SAF2017-88908-R) and PT17/0009/0006 from the ISCIII (C.Ç. and J.D.B.); the Academy of Finland (grants 259926, 265204, 292839, 314456, and 335446), the Paulo Foundation, the Finnish Cultural Foundation Southwest Finland Regional Fund, the Turku University Hospital Research Funds, and the European Union (EUFP7 project 278373; DIABAT) (K.A.V. and M.U.-D.); the Fundación Ramón Areces (BEVP32P01S10090) and subsequently by a Sir Henry Wellcome postdoctoral fellowship (222748/Z/21/Z) (S.R.-F.); We thank the Wellcome-Trust Sanger Institute Mouse Genetics Project (Sanger MGP) and its funders for providing the mutant mouse line (Pepd<tm1a[KOMP]Wtsi). Funding and associated primary phenotypic information may be found at www.sanger.ac.uk/mouseportal. We thank Dr. Guillaume Bidault for his scientific and technical advice. The PAZ6 cell line was a gift from Dr. Tarik Issad, Institute Cochin, Paris, France. Immortalized murine primary brown adipocytes (pBATs) were kindly provided by Prof. Francesc Villarroya (University of Barcelona, Spain). We thank Prof. Martin Klingenspor and Dr. Tobias Fromme from the Technical University of Munich (Freising, Germany) for accessing the human RNA-seq data. The funders had no role in study design, data collection and interpretation, or submitting the work for publication. Please note that the authors' views are those and not necessarily those of the National Health Service (NHS), the National Institute for Health and Care Research (NIHR), or the Department of Health and Social Care.

AUTHOR CONTRIBUTIONS

Conceptualization, V.P., and A.V.-P.; Methodology, V.P.; Investigation, V.P., E.F.-J., I.S., S.R.-F., and J.L.; Formal Analysis, V.P. , E.F.-J., I.S., S.R.-F., M.U.-D., S.V., C.Ç., J.L., and J.D.B.; Resources, M.U.-D, V.J.P., T.N., M.C., S.R.-C., S.C., and K.A.V.; Writing – Original Draft, V.P., I.S., and A.V.-P.; Writing – Review & Editing, V.P. and A.V.-P.; Supervision, A.V.-P.; Project Administration, M.C. and A.V.-P.; Funding Acquisition, A.V.-P.

DECLARATION OF INTERESTS

The authors declare no competing interests.

INCLUSION AND DIVERSITY

We support inclusive, diverse, and equitable conduct of research.

Received: January 3, 2023
Revised: April 25, 2023
Accepted: May 29, 2023
Published: June 13, 2023

REFERENCES

1. Wibmer, A.G., Becher, T., Eljalby, M., Crane, A., Andrieu, P.C., Jiang, C.S., Vaughan, R., Schöder, H., and Cohen, P. (2021). Brown adipose tissue is associated with healthier body fat distribution and metabolic benefits independent of regional adiposity. Cell Rep. Med. *2*, 100332. https://doi.org/10.1016/j.xcrm.2021.100332.
2. Herz, C.T., Kulterer, O.C., Prager, M., Schmöltzer, C., Langer, F.B., Prager, G., Marculescu, R., Kautzky-Willer, A., Hacker, M., Haug, A.R., and Kiefer, F.W. (2021). Active Brown adipose tissue is associated with a healthier metabolic phenotype in obesity. Diabetes *71*, 93–103, db210475.. https://doi.org/10.2337/db21-0475
3. Kulterer, O.C., Herz, C.T., Prager, M., Schmöltzer, C., Langer, F.B., Prager, G., Marculescu, R., Kautzky-Willer, A., Hacker, M., Haug, A.R., and Kiefer, F.W. (2022). Brown adipose tissue prevalence is lower in obesity but its metabolic activity is intact. Front. Endocrinol. *13*, 858417. https://doi.org/10.3389/fendo.2022.858417.
4. Leitner, B.P., Huang, S., Brychta, R.J., Duckworth, C.J., Baskin, A.S., McGehee, S., Tal, I., Dieckmann, W., Gupta, G., Kolodny, G.M., et al. (2017). Mapping of human brown adipose tissue in lean and obese young men. Proc. Natl. Acad. Sci. USA *114*, 8649–8654. https://doi.org/10.1073/pnas.1705287114.
5. Sakamoto, T., Nitta, T., Maruno, K., Yeh, Y.-S., Kuwata, H., Tomita, K., Goto, T., Takahashi, N., and Kawada, T. (2016). Macrophage infiltration into obese adipose tissues suppresses the induction of UCP1 level in mice. Am. J. Physiol. Endocrinol. Metab. *310*, E676–E687. https://doi.org/10.1152/ajpendo.00028.2015.
6. Villarroya, F., Cereijo, R., Gavaldà-Navarro, A., Villarroya, J., and Giralt, M. (2018). Inflammation of brown/beige adipose tissues in obesity and metabolic disease. J. Intern. Med. *284*, 492–504. https://doi.org/10.1111/joim.12803.
7. Bae, J., Ricciardi, C.J., Esposito, D., Komarnytsky, S., Hu, P., Curry, B.J., Brown, P.L., Gao, Z., Biggerstaff, J.P., Chen, J., and Zhao, L. (2014). Activation of pattern recognition receptors in Brown adipocytes induce inflammation and suppress uncoupling protein 1 expression and mitochondrial respiration. Am. J. Physiol. Cell Physiol. *306*, C918–C930. https://doi.org/10.1152/ajpcell.00249.2013.
8. Sun, K., Tordjman, J., Clément, K., and Scherer, P.E. (2013). Fibrosis and adipose tissue dysfunction. Cell Metabol. *18*, 470–477. https://doi.org/10.1016/j.cmet.2013.06.016.
9. Ruiz-Ojeda, F.J., Méndez-Gutiérrez, A., Aguilera, C.M., and Plaza-Díaz, J. (2019). Extracellular matrix remodeling of adipose tissue in obesity and metabolic diseases. Int. J. Mol. Sci. *20*, 4888. https://doi.org/10.3390/ijms20194888.
10. Divoux, A., and Clément, K. (2011). Architecture and the extracellular matrix: the still unappreciated components of the adipose tissue. Obes. Rev. *12*, e494–e503. https://doi.org/10.1111/j.1467-789X.2010.00811.x.
11. Bonnans, C., Chou, J., and Werb, Z. (2014). Remodelling the extracellular matrix in development and disease. Nat. Rev. Mol. Cell Biol. *15*, 786–801. https://doi.org/10.1038/nrm3904.
12. Kitchener, R.L., and Grunden, A.M. (2012). Prolidase function in proline metabolism and its medical and biotechnological applications. J. Appl. Microbiol. *113*, 233–247. https://doi.org/10.1111/j.1365-2672.2012.05310.x.
13. Wynn, T.A., and Ramalingam, T.R. (2012). Mechanisms of fibrosis: therapeutic translation for fibrotic disease. Nat. Med. *18*, 1028–1040. https://doi.org/10.1038/nm.2807.
14. Pellegrinelli, V., Carobbio, S., and Vidal-Puig, A. (2016). Adipose tissue plasticity: how fat depots respond differently to pathophysiological cues. Diabetologia *59*, 1075–1088. https://doi.org/10.1007/s00125-016-3933-4.
15. DeBari, M.K., and Abbott, R.D. (2020). Adipose tissue fibrosis: mechanisms, models, and importance. Int. J. Mol. Sci. *21*, 6030. https://doi.org/10.3390/ijms21176030.
16. Pellegrinelli, V., Heuvingh, J., du Roure, O., Rouault, C., Devulder, A., Klein, C., Lacasa, M., Clément, E., Lacasa, D., and Clément, K. (2014). Human adipocyte function is impacted by mechanical cues. J. Pathol. *233*, 183–195. https://doi.org/10.1002/path.4347.
17. Villarroya, J., Cereijo, R., Giralt, M., and Villarroya, F. (2019). Secretory proteome of Brown adipocytes in response to cAMP-mediated thermogenic

activation. Front. Physiol. *10*, 67. https://doi.org/10.3389/fphys.2019.00067.

18. Li, Y., Wang, X., Wang, F., You, L., Xu, P., Cao, Y., Chen, L., Wen, J., Guo, X., Cui, X., and Ji, C. (2019). Identification of intracellular peptides associated with thermogenesis in human brown adipocytes. J. Cell. Physiol. *234*, 7104–7114. https://doi.org/10.1002/jcp.27465.
19. Gonzalez Porras, M.A., Stojkova, K., Vaicik, M.K., Pelowe, A., Goddi, A., Carmona, A., Long, B., Qutub, A.A., Gonzalez, A., Cohen, R.N., and Brey, E.M. (2021). Integrins and extracellular matrix proteins modulate adipocyte thermogenic capacity. Sci. Rep. *11*, 5442. https://doi.org/10.1038/s41598-021-84828-z.
20. Grandoch, M., Flögel, U., Virtue, S., Maier, J.K., Jelenik, T., Kohlmorgen, C., Feldmann, K., Ostendorf, Y., Castañeda, T.R., Zhou, Z., et al. (2019). 4-Methylumbelliferone improves the thermogenic capacity of brown adipose tissue. Nat. Metab. *1*, 546–559. https://doi.org/10.1038/s42255-019-0055-6.
21. Sun, K., Park, J., Gupta, O.T., Holland, W.L., Auerbach, P., Zhang, N., Goncalves Marangoni, R., Nicoloro, S.M., Czech, M.P., Varga, J., et al. (2014). Endotrophin triggers adipose tissue fibrosis and metabolic dysfunction. Nat. Commun. *5*, 3485. https://doi.org/10.1038/ncomms4485.
22. Bagchi, M., Kim, L.A., Boucher, J., Walshe, T.E., Kahn, C.R., and D'Amore, P.A. (2013). Vascular endothelial growth factor is important for brown adipose tissue development and maintenance. Faseb. J. *27*, 3257–3271. https://doi.org/10.1096/fj.12-221812.
23. Rangel-Azevedo, C., Santana-Oliveira, D.A., Miranda, C.S., Martins, F.F., Mandarim-de-Lacerda, C.A., and Souza-Mello, V. (2022). Progressive brown adipocyte dysfunction: whitening and impaired nonshivering thermogenesis as long-term obesity complications. J. Nutr. Biochem. *105*, 109002. https://doi.org/10.1016/j.jnutbio.2022.109002.
24. Shimizu, I., Aprahamian, T., Kikuchi, R., Shimizu, A., Papanicolaou, K.N., MacLauchlan, S., Maruyama, S., and Walsh, K. (2014). Vascular rarefaction mediates whitening of brown fat in obesity. J. Clin. Invest. *124*, 2099–2112. https://doi.org/10.1172/JCI71643.
25. Martins, F.F., Bargut, T.C.L., Aguila, M.B., and Mandarim-de-Lacerda, C.A. (2017). Thermogenesis, fatty acid synthesis with oxidation, and inflammation in the brown adipose tissue of ob/ob (−/−) mice. Annals of Anatomy - Anatomischer Anzeiger *210*, 44–51. https://doi.org/10.1016/j.aanat.2016.11.013.
26. Kotzbeck, P., Giordano, A., Mondini, E., Murano, I., Severi, I., Venema, W., Cecchini, M.P., Kershaw, E.E., Barbatelli, G., Haemmerle, G., et al. (2018). Brown adipose tissue whitening leads to brown adipocyte death and adipose tissue inflammation. J. Lipid Res. *59*, 784–794. https://doi.org/10.1194/jlr.M079665.
27. Alcalá, M., Calderon-Dominguez, M., Bustos, E., Ramos, P., Casals, N., Serra, D., Viana, M., and Herrero, L. (2017). Increased inflammation, oxidative stress and mitochondrial respiration in brown adipose tissue from obese mice. Sci. Rep. *7*, 16082. https://doi.org/10.1038/s41598-017-16463-6.
28. Wang, H., Willershäuser, M., Li, Y., Fromme, T., Schnabl, K., Bast-Habersbrunner, A., Ramisch, S., Mocek, S., and Klingenspor, M. (2021). Uncoupling protein-1 expression does not protect mice from diet-induced obesity. Am. J. Physiol. Endocrinol. Metab. *320*, E333–E345. https://doi.org/10.1152/ajpendo.00285.2020.
29. Dieckmann, S., Strohmeyer, A., Willershäuser, M., Maurer, S.F., Wurst, W., Marschall, S., de Angelis, M.H., Kühn, R., Worthmann, A., Fuh, M.M., et al. (2022). Susceptibility to diet-induced obesity at thermoneutral conditions is independent of UCP1. Am. J. Physiol. Endocrinol. Metab. *322*, E85–E100. https://doi.org/10.1152/ajpendo.00278.2021.
30. Feldmann, H.M., Golozoubova, V., Cannon, B., and Nedergaard, J. (2009). UCP1 ablation induces obesity and abolishes diet-induced thermogenesis in mice exempt from thermal stress by living at thermoneutrality. Cell Metabol. *9*, 203–209. https://doi.org/10.1016/j.cmet.2008.12.014.
31. Cui, X., Nguyen, N.L.T., Zarebidaki, E., Cao, Q., Li, F., Zha, L., Bartness, T., Shi, H., and Xue, B. (2016). Thermoneutrality decreases thermogenic program and promotes adiposity in high-fat diet-fed mice. Phys. Rep. *4*, e12799. https://doi.org/10.14814/phy2.12799.
32. Mills, E.L., Harmon, C., Jedrychowski, M.P., Xiao, H., Garrity, R., Tran, N.V., Bradshaw, G.A., Fu, A., Szpyt, J., Reddy, A., et al. (2021). UCP1 governs liver extracellular succinate and inflammatory pathogenesis. Nat. Metab. *3*, 604–617. https://doi.org/10.1038/s42255-021-00389-5.
33. Cao, J., Zhu, Q., Liu, L., Glazier, B.J., Hinkel, B.C., Liang, C., and Shi, H. (2018). Global transcriptome analysis of Brown adipose tissue of diet-induced obese mice. IJMS *19*, 1095. https://doi.org/10.3390/ijms19041095.
34. Cannon, B., and Nedergaard, J. (2004). Brown adipose tissue: function and physiological significance. Physiol. Rev. *84*, 277–359. https://doi.org/10.1152/physrev.00015.2003.
35. Wang, Y., Li, X., Liu, C., Zhou, L., Shi, L., Zhang, Z., Chen, L., Gao, M., Gao, L., Xu, Y., et al. (2022). WTAP regulates postnatal development of brown adipose tissue by stabilizing METTL3 in mice. Life Metab. *1*, 270–284. https://doi.org/10.1093/lifemeta/loac028.
36. Sun, W., Dong, H., Balaz, M., Slyper, M., Drokhlyansky, E., Colleluori, G., Giordano, A., Kovanicova, Z., Stefanicka, P., Balazova, L., et al. (2020). snRNA-seq reveals a subpopulation of adipocytes that regulates thermogenesis. Nature *587*, 98–102. https://doi.org/10.1038/s41586-020-2856-x.
37. Pellegrinelli, V., Rodriguez-Cuenca, S., Rouault, C., Figueroa-Juarez, E., Schilbert, H., Virtue, S., Moreno-Navarrete, J.M., Bidault, G., Vázquez-Borrego, M.C., Dias, A.R., et al. (2022). Dysregulation of macrophage PEPD in obesity determines adipose tissue fibro-inflammation and insulin resistance. Nat. Metab. *4*, 476–494. https://doi.org/10.1038/s42255-022-00561-5.
38. Klein, J., Fasshauer, M., Klein, H.H., Benito, M., and Kahn, C.R. (2002). Novel adipocyte lines from brown fat: a model system for the study of differentiation, energy metabolism, and insulin action. Bioessays *24*, 382–388. https://doi.org/10.1002/bies.10058.
39. Frantz, C., Stewart, K.M., and Weaver, V.M. (2010). The extracellular matrix at a glance. J. Cell Sci. *123*, 4195–4200. https://doi.org/10.1242/jcs.023820.
40. Yang, S., and Plotnikov, S.V. (2021). Mechanosensitive regulation of fibrosis. Cells *10*, 994. https://doi.org/10.3390/cells10050994.
41. Virtue, S., and Vidal-Puig, A. (2013). Assessment of brown adipose tissue function. Front. Physiol. *4*, 128. https://doi.org/10.3389/fphys.2013.00128.
42. U Din, M., Saari, T., Raiko, J., Kudomi, N., Maurer, S.F., Lahesmaa, M., Fromme, T., Amri, E.-Z., Klingenspor, M., Solin, O., et al. (2018). Postprandial oxidative metabolism of human Brown fat indicates thermogenesis. Cell Metabol. *28*, 207–216.e3. https://doi.org/10.1016/j.cmet.2018.05.020.
43. Zilberfarb, V., Piétri-Rouxel, F., Jockers, R., Krief, S., Delouis, C., Issad, T., and Strosberg, A.D. (1997). Human immortalized brown adipocytes express functional beta3-adrenoceptor coupled to lipolysis. J. Cell Sci. *110* (*Pt 7*), 801–807.
44. LeBleu, V.S., Macdonald, B., and Kalluri, R. (2007). Structure and function of basement membranes. Exp. Biol. Med. (Maywood) *232*, 1121–1129. https://doi.org/10.3181/0703-MR-72.
45. Mariman, E.C.M., and Wang, P. (2010). Adipocyte extracellular matrix composition, dynamics and role in obesity. Cell. Mol. Life Sci. *67*, 1277–1292. https://doi.org/10.1007/s00018-010-0263-4.
46. Tran, K.-V., Brown, E.L., DeSouza, T., Jespersen, N.Z., Nandrup-Bus, C., Yang, Q., Yang, Z., Desai, A., Min, S.Y., Rojas-Rodriguez, R., et al. (2020). Human thermogenic adipocyte regulation by the long noncoding RNA LINC00473. Nat. Metab. *2*, 397–412. https://doi.org/10.1038/s42255-020-0205-x.
47. Sanchez-Gurmaches, J., Tang, Y., Jespersen, N.Z., Wallace, M., Martinez Calejman, C., Gujja, S., Li, H., Edwards, Y.J.K., Wolfrum, C., Metallo, C.M., et al. (2018). Brown fat AKT2 is a cold-induced kinase that stimulates ChREBP-mediated de novo lipogenesis to optimize fuel storage and

thermogenesis. Cell Metabol. *27*, 195–209.e6. https://doi.org/10.1016/j.cmet.2017.10.008.

48. Madsen, D.H., Leonard, D., Masedunskas, A., Moyer, A., Jürgensen, H.J., Peters, D.E., Amornphimoltham, P., Selvaraj, A., Yamada, S.S., Brenner, D.A., et al. (2013). M2-like macrophages are responsible for collagen degradation through a mannose receptor-mediated pathway. J. Cell Biol. *202*, 951–966. https://doi.org/10.1083/jcb.201301081.
49. Campderrós, L., Moure, R., Cairó, M., Gavaldà-Navarro, A., Quesada-López, T., Cereijo, R., Giralt, M., Villarroya, J., and Villarroya, F. (2019). Brown adipocytes secrete GDF15 in response to thermogenic activation. Obesity *27*, 1606–1616. https://doi.org/10.1002/oby.22584.
50. Quesada-López, T., Cereijo, R., Turatsinze, J.-V., Planavila, A., Cairó, M., Gavaldà-Navarro, A., Peyrou, M., Moure, R., Iglesias, R., Giralt, M., et al. (2016). The lipid sensor GPR120 promotes brown fat activation and FGF21 release from adipocytes. Nat. Commun. *7*, 13479. https://doi.org/10.1038/ncomms13479.
51. Keijer, J., Li, M., and Speakman, J.R. (2019). What is the best housing temperature to translate mouse experiments to humans? Mol. Metabol. *25*, 168–176. https://doi.org/10.1016/j.molmet.2019.04.001.
52. Halberg, N., Khan, T., Trujillo, M.E., Wernstedt-Asterholm, I., Attie, A.D., Sherwani, S., Wang, Z.V., Landskroner-Eiger, S., Dineen, S., Magalang, U.J., et al. (2009). Hypoxia-inducible factor 1alpha induces fibrosis and insulin resistance in white adipose tissue. Mol. Cell Biol. *29*, 4467–4483. https://doi.org/10.1128/MCB.00192-09.
53. Strissel, K.J., Stancheva, Z., Miyoshi, H., Perfield, J.W., 2nd, DeFuria, J., Jick, Z., Greenberg, A.S., and Obin, M.S. (2007). Adipocyte death, adipose tissue remodeling, and obesity complications. Diabetes *56*, 2910–2918. https://doi.org/10.2337/db07-0767.
54. Spencer, M., Yao-Borengasser, A., Unal, R., Rasouli, N., Gurley, C.M., Zhu, B., Peterson, C.A., and Kern, P.A. (2010). Adipose tissue macrophages in insulin-resistant subjects are associated with collagen VI and fibrosis and demonstrate alternative activation. Am. J. Physiol. Endocrinol. Metab. *299*, E1016–E1027. https://doi.org/10.1152/ajpendo.00329.2010.
55. Keophiphath, M., Achard, V., Henegar, C., Rouault, C., Clément, K., and Lacasa, D. (2009). Macrophage-secreted factors promote a profibrotic phenotype in human preadipocytes. Mol. Endocrinol. *23*, 11–24. https://doi.org/10.1210/me.2008-0183.
56. Hepler, C., Shan, B., Zhang, Q., Henry, G.H., Shao, M., Vishvanath, L., Ghaben, A.L., Mobley, A.B., Strand, D., Hon, G.C., and Gupta, R.K. (2018). Identification of functionally distinct fibro-inflammatory and adipogenic stromal subpopulations in visceral adipose tissue of adult mice. Elife *7*, e39636. https://doi.org/10.7554/eLife.39636.
57. Marcelin, G., Ferreira, A., Liu, Y., Atlan, M., Aron-Wisnewsky, J., Pelloux, V., Botbol, Y., Ambrosini, M., Fradet, M., Rouault, C., et al. (2017). A PDGFRα-mediated switch toward CD9(high) adipocyte progenitors controls obesity-induced adipose tissue fibrosis. Cell Metabol. *25*, 673–685. https://doi.org/10.1016/j.cmet.2017.01.010.
58. Kaiyala, K.J., and Schwartz, M.W. (2011). Toward a more complete (and less controversial) understanding of energy expenditure and its role in obesity pathogenesis. Diabetes *60*, 17–23. https://doi.org/10.2337/db10-0909.
59. Marette, A., Deshaies, Y., Collet, A.J., Tulp, O., and Bukowiecki, L.J. (1991). Major thermogenic defect associated with insulin resistance in brown adipose tissue of obese diabetic SHR/N-cp rats. Am. J. Physiol. *261*, E204–E213. https://doi.org/10.1152/ajpendo.1991.261.2.E204.
60. Khan, T., Muise, E.S., Iyengar, P., Wang, Z.V., Chandalia, M., Abate, N., Zhang, B.B., Bonaldo, P., Chua, S., and Scherer, P.E. (2009). Metabolic dysregulation and adipose tissue fibrosis: role of collagen VI. Mol. Cell Biol. *29*, 1575–1591. https://doi.org/10.1128/MCB.01300-08.
61. Hasegawa, Y., Ikeda, K., Chen, Y., Alba, D.L., Stifler, D., Shinoda, K., Hosono, T., Maretich, P., Yang, Y., Ishigaki, Y., et al. (2018). Repression of adipose tissue fibrosis through a PRDM16-GTF2IRD1 complex improves systemic glucose homeostasis. Cell Metabol. *27*, 180–194.e6. https://doi.org/10.1016/j.cmet.2017.12.005.
62. Carobbio, S., Guenantin, A.-C., Bahri, M., Rodriguez-Fdez, S., Honig, F., Kamzolas, I., Samuelson, I., Long, K., Awad, S., Lukovic, D., et al. (2021). Unraveling the developmental roadmap toward human Brown AdiposeTissue. Stem Cell Rep. *16*, 1010. https://doi.org/10.1016/j.stemcr.2021.03.009.
63. Miranda, S., González-Rodríguez, A., Revuelta-Cervantes, J., Rondinone, C.M., and Valverde, A.M. (2010). Beneficial effects of PTP1B deficiency on brown adipocyte differentiation and protection against apoptosis induced by pro- and anti-inflammatory stimuli. Cell. Signal. *22*, 645–659. https://doi.org/10.1016/j.cellsig.2009.11.019.
64. Orava, J., Nuutila, P., Lidell, M.E., Oikonen, V., Noponen, T., Viljanen, T., Scheinin, M., Taittonen, M., Niemi, T., Enerbäck, S., and Virtanen, K.A. (2011). Different metabolic responses of human brown adipose tissue to activation by cold and insulin. Cell Metabol. *14*, 272–279. https://doi.org/10.1016/j.cmet.2011.06.012.
65. Whittle, A.J., Carobbio, S., Martins, L., Slawik, M., Hondares, E., Vázquez, M.J., Morgan, D., Csikasz, R.I., Gallego, R., Rodriguez-Cuenca, S., et al. (2012). BMP8B increases brown adipose tissue thermogenesis through both central and peripheral actions. Cell *149*, 871–885. https://doi.org/10.1016/j.cell.2012.02.066.
66. Pellegrinelli, V., Rodriguez-Cuenca, S., Rouault, C., Schilbert, H., Virtue, S., Moreno-Navarrete, J.M., Bidault, G., Borrego, M., del, C.V., Dias, A.R., Pucker, B., et al. (2020). Dysregulation of macrophage PEPD in obesity determines adipose tissue fibro-inflammation and insulin resistance, Review. https://doi.org/10.21203/rs.3.rs-57182/v1.
67. Lacasa, D., Taleb, S., Keophiphath, M., Miranville, A., and Clement, K. (2007). Macrophage-secreted factors impair human adipogenesis: involvement of proinflammatory state in preadipocytes. Endocrinology *148*, 868–877. https://doi.org/10.1210/en.2006-0687.
68. Pellegrinelli, V., Peirce, V.J., Howard, L., Virtue, S., Türei, D., Senzacqua, M., Frontini, A., Dalley, J.W., Horton, A.R., Bidault, G., et al. (2018). Adipocyte-secreted BMP8b mediates adrenergic-induced remodeling of the neuro-vascular network in adipose tissue. Nat. Commun. *9*, 4974. https://doi.org/10.1038/s41467-018-07453-x.
69. Metsalu, T., and Vilo, J. (2015). ClustVis: a web tool for visualizing clustering of multivariate data using Principal Component Analysis and heatmap. Nucleic Acids Res. *43*, W566–W570. https://doi.org/10.1093/nar/gkv468.

STAR★METHODS

KEY RESOURCES TABLE

REAGENT or RESOURCE	SOURCE	IDENTIFIER
Antibodies		
Anti-collagen I	Abcam	Cat# ab21286; RRID:AB_446161
Anti-collagen III	Abcam	Cat# ab7778; RRID:AB_306066
Anti-collagen IV	Abcam	Cat# ab6586; RRID:AB_305584
Anti-collagen V	Abcam	Cat# ab7046, RRID:AB_305723
Anti-collagen VI	Abcam	Cat# ab182744, RRID:AB_284791
Anti-fibronectin	Abcam	Cat# ab2413, RRID:AB_2262874
MACS mouse CD11b microbeads	Miltnyibiotec	Cat# 130-049-601, RRID:N/A
MACS mouse CD45 microbeads	Miltnyibiotec	Cat# 130-052-301, RRID:N/A
MACS mouse CD31 microbeads	Miltnyibiotec	Cat# 130-097-418, RRID:N/A
Alexa 555-conjugated anti-rabbit	Life Technologies	Cat# A-21428, RRID:AB_2535849
Alexa 488-conjugated anti-mouse	Life technologies	Cat# A-21202, RRID:AB_141607
Chemicals, peptides, and recombinant proteins		
Lipopolysaccharide	Sigma-aldrich	Cat# L4391
(±)-Norepinephrine (+)-bitartrate salt	Sigma	Cat# A0937-5G
Insulin (Actrapid 100 IU/mL)	Novo Nordisk	Cat# 1331415
Bodipy 493/503	Life science	Cat# D-3922
Phalloidin-iFluor 594 Reagent	Abcam	Cat# ab176757
Hoechst 33342	Thermofisher	Cat# H3570
PuraMatrix® hydrogel	Corning Life Science	Cat# 354250
45% HFD 58% HFD	Research Diets	Cat# D12451 Cat# 12331
Triton X-100	Sigma-aldrich	Cat# T-9284
STAT60	AMS Biotechnology	Cat# CS-502
Collagenase from Clostridium histolyticum type 2	Sigma-aldrich	Cat# C6885
Bovine serum albumin	Sigma-aldrich	Cat# A8412
Critical commercial assays		
Free glycerol assay	Sigma-aldrich	Cat# F6428-40mL
RNeasy minikit (250)	Qiagen	Cat# 74106
RNA 6000 Nano Kit	Agilent	Cat# 5067–1511
TruSeq Stranded mRNA HT Sample Prep Kit	Illumina	Cat# 20020595
Proteome Profiler Mouse Angiogenesis Array Kit	R&D Systems	Cat# ARY015
Deposited data		
Single nuclei RNAseq: murine BAT	Y Wang et al.[35]	GEO: GSE202630
Single nuclei RNAseq: human BAT	W Sun et al.[36]	EBI: E-MTAB-8564
RNAseq data: human NE-treated adipocytes	KV Tran et al.[46]	N/A
RNAseq data: PAZ6 adipocytes	SC and ACG et al.[62]	GEO: GSE168387
RNAseq data: mice exposed to cold and TN	J Sanchez-Gurmaches et al.[47]	GEO: GSE96681
Human RNAseq data	M U-Din et al.[42]	GEO: GSE113764
Experimental models: Cell lines		
Murine immortalised brown preadipocyte cells (C57BAT).	Laboratory of Dr. C. Ronald Kahn[38]	N/A
Murine immortalised brown preadipocyte cells (pBAT)	Laboratory of Dr. Ángela M. Valverde[63]	N/A
Human immortalised brown preadipocyte cells (PAZ6)	Laboratory of Dr. Tarik Issad[43]	N/A

(*Continued on next page*)

Continued

REAGENT or RESOURCE	SOURCE	IDENTIFIER
Experimental models: Organisms/strains		
C57Bl/6J	Charles River	JAX™ Strain, RRID:IMSR_JAX:000664
C57BL/6J-Lepob	Charles River	JAX™ Strain, RRID:IMSR_JAX: 000632
Pepdtm1a(KOMP)Wtsi	Wellcome Trust Sanger Institute	MFPW; EPD0224_1_C04
Software and algorithms		
GraphPad Prism7 and 8	GraphPad Software	RRID: SCR_002798
Fiji	Fiji	RRID: SCR_002285
Zeiss LSM 510 Meta Confocal microscope with LSM 3D software	Carl Zeiss	N/A

RESOURCE AVAILABILITY

Lead contact

Further information and requests for resources and reagents should be directed to and will be fulfilled by the lead contact, Antonio Vidal-Puig (ajv22@medschl.cam.ac.uk).

Materials availability

This study did not generate new unique reagents.

Data and code availability

- This paper analyzes existing publicly available data. These accession numbers for the datasets are listed in the key resources table.
- This paper does not report original code.
- Any additional information required to reanalyze the data reported in this paper is available from the lead contact, Antonio Vidal-Puig (ajv22@medschl.cam.ac.uk), upon request.

EXPERIMENTAL MODEL AND STUDY PARTICIPANT DETAILS

Animal models

8-10 weeks old male C57Bl6/J mice were purchased from Charles River. *Pepd* WT and HET mice were generated by the Wellcome Trust Sanger Institute Mouse Genetics Project on a C57Bl6/J background by mating HET mice. *Pepd*-homozygous and *Pepd*-HET pups were born at expected Mendelian ratios. In line with the 3R, only a subpopulation of the pups born was selected for each study. 8–10 weeks old male *Pepd* WT and HET were used for each experiment. Wild-type $Lep^{wt/wt}$ and leptin-deficient mice, $Lep^{ob/ob}$, were on a C57BL/6 background. Studies were conducted in 8–28 weeks-old mice using littermate controls. This research has been regulated under the Animals (Scientific Procedures) Act 1986 Amendment Regulations 2012 following ethical review by the University of Cambridge Animal Welfare and Ethical Review Body (AWERB) under pathogen-free conditions and housed according to UK Home Office guidelines and carried out by the Disease Model Core unit. Animals were housed in 3–4 per cage in a temperature-controlled room (22°C) with a 12-h light/dark cycle, with 55% relative humidity and ad libitum access to food and water. A standard chow diet (DS-105, Safe Diets) was administered to all animals from weaning, consisting of 64.3% carbohydrate, 22.4% protein and 13.3% lipid of total calories. Only male mice were used for *in vivo* and *in vitro* experiments, isolation of primary cells preparation of BMDMs.

Generation of bone marrow chimeras

C57BL6/J mice at 10 weeks of age received a sublethal dose of whole-body irradiation (9Gy). The day after irradiation, donor *Pepd* KO mice were culled, and their femurs and tibias were removed aseptically. Marrow cavities were flushed in RPMI medium, and single-cell suspensions were prepared. The irradiated recipients received 1×10^7 bone marrow cells in 0.1mL of PBS by tail-vein injection. During 4 weeks after BMT, Bactrim (Roche) was added to drinking water. After two additional weeks, mice were switched to a 58% HFD. Mice were culled 16 weeks later to collect blood and tissues.

Temperature studies

Chow-fed male C57Bl/6 WT mice were kept at room temperature (RT, 21°C), and acclimated (3 weeks) to 8°C (CE) or thermoneutrality (30C, TN). Before moving to the appropriate housing temperature, all mice had previously been housed at 21°C, and all mice were 18 weeks old when culled.

HFD studies

Diets for animal studies included standard chow (10% calories from lipid), HFD 45% (D12451, Research Diets, 45% calories from lipid) and HFD 58% (D12331, Research Diets, 58% calories from lipid). Standard chow or HFD was provided ad libitum to animals from 8 weeks old until indicated.

Body composition

Fat and lean masses were calculated by time-domain nuclear magnetic resonance (TD-NMR) by using a minispec Live Mice Analyzer LF50 (Bruker).

Human subjects

Paired biopsies of BAT and WAT were obtained from the supraclavicular region of 14 healthy subjects of both sexes (10 females and 4 males) with the approval of ethical review board of the Hospital District of Southwest Finland. All enrolled study subjects were non-diabetic, had normal oral glucose tolerance test, healthy cardiovascular status and level of circulatory hepatic enzymes within adequate range. Informed written consent was obtained from all study subjects prior to inclusion in the study. The study was carried out according to the principles of declaration of Helsinki and GCP guidelines. The anthropometric characteristics of this study cohort are shown in Table 1. The procedure was carried out at room temperature ($\sim 22^{\circ}C$) under local lidocaine-epinephrine anesthesia by an experienced plastic surgeon using available imaging data of BAT location. The WAT sample was collected from the same incision. The adipose tissue samples were snap-frozen in liquid nitrogen immediately after the excision. RNA Isolation and Next Generation Sequencing were performed as described in.[42]. [^{18}F]FDG PET or [^{18}F]FTHA PET imaging under the cold exposure was performed as previously described.[42,64] More details regarding participants and original study are found in.[42]

Cell culture

Murine brown adipocyte cell lines

C57BAT and pBAT brown preadipocyte cell lines were used for *in vitro* experiments. Both immortalized cell line were generated from SVF cells of interscapular BAT from newborn mice (sexes not reported) and differentiated as previously described.[38,63,65] For 2D cultures, cells were plated 50,000 cells/12 well plates and maintained in a differentiation medium until fully differentiated. By day 8 (C57BAT) or 6 (pBAT) post-induction, cells were defined as differentiated if they appeared healthy and lipid replete. Cells were kept either in normoxic conditions (21% O_2) or, after 24 h, switched to hypoxic conditions (5% O_2).

Human brown adipocyte cell line

The human immortalised brown preadipocyte cell line Paz6 was generated from SVF cells of an infant brown adipose tissue (sex not reported) and differentiated to adipocytes as described previously.[43]

Primary brown adipocytes

Brown adipose tissue from 8 weeks old male C57Bl/6 WT and Pepd HET mice was dissected from the interscapular region, cut into small pieces, and incubated for 40 min at 37°C in digestion media containing 1 mg/ml of Collagenase II and 1% BSA in FBS-free DMEM/F12 medium. Digestion was stopped with 1/5 volume of FBS, and the mixture was filtered through a 100 μm cell strainer before centrifugation at 300 x g for 5 min. The upper phase containing the mature adipocytes was collected, and the remaining cells were centrifuged at 600 x g for 5 min. The pellet was resuspended in 1x red blood cell (RBC) lysis buffer (ThermoFisher Scientific) and incubated for 4 min on ice. Primary brown adipocytes culture medium (PBACM) containing DMEM/F12 10% FBS, 1% L-glutamine and 1% Penicillin-Streptomycin was added to the cells before centrifugation at 600 x g for 5 min. The pellet (stromal vascular fraction, SVF) was resuspended in PBACM and cultured in T25 flasks. After 24h, cells were washed with PBS to remove floating cells, and a fresh culture medium was added. Cells were maintained in this manner with the medium changed every 2 days until differentiation after two passages. Cells were then seeded in 12-well plates (5 x 10^5 cells) until 80% confluence. The medium was then changed to "induction medium" (day 0), containing PBACM 0.5mM IBMX, 1uM dexamethasone, 1ug/ml insulin, 1uM rosiglitazone and 1nM T3. After 48h, the induction medium was replaced with a "maintenance medium" containing PBACM 1ug/μl insulin and 1nM T3. The maintenance medium was changed every two days until complete differentiation (about 7days). On day 7, primary differentiated adipocyte cells were activated with norepinephrine (NE) 1μM for 6h.

Culture with conditioned medium from activated macrophages

Bone marrow from the femur and tibia bones from 10 to 16 weeks-old C57BL6 WT mice was collected, and bone marrow-derived macrophages (BMDMs) were prepared as previously described.[66] After differentiation, BMDMs were cultured in 12 well-culture plates (5 X 10^5 cells) for 24h in BMDM medium before 6h stimulation with LPS (100 ng/ml). Activated BMDMs were then cultured in fresh media for 24h. Conditioned media was collected, centrifuged to eliminate cell debris and stored at −80°C. C57BAT preadipocytes were differentiated in 3V DMEM with 10% fetal bovine serum (F.B.S.) and containing the adipogenic cocktail[65] with 1V control RPMI or conditioned media from activated macrophages CM M(LPS) as previously described[67] for 9 days. For immunofluorescence analysis, C57BAT preadipocytes were differentiated on glass coverslips with or without CM M(LPS) for 9 days, as mentioned above.

3D culture of brown adipocytes with ECM from lean and obese mice

Before 3D culture, ECM from either lean *Lep*$^{wt/wt}$ or obese *Lep*$^{Ob/Ob}$ mice was minced finely and mixed with Puramatrix hydrogel at a 0.25 g/mL concentration, corresponding to the proportion of fibrosis/adipocytes observed in adipose tissue from obese subjects.[16] The mixture was sonicated for 30 min and minced once more before diluting 1:1 20% sucrose solution. pBAT cells were collected,

resuspended in 10%sucrose and embedded into the hydrogel alone (control 3D condition) or in the presence of ECM at a 1:1 ratio for a final concentration of 1000cells/μL and 0.0625g ECM/mL. 300μL of cell mixture was incorporated into 24-well plates containing 1mL of prewarmed serum-free medium. After 1h at 37C, the medium was changed to a differentiation medium. Cells were differentiated as previously described for 6 days.[38] Briefly, cells were maintained in a growth medium (DMEM 10% FBS with L-glutamine and pen-strep). Cells were fed a differentiation medium every two days (growth medium with T3 and insulin) for differentiation. When confluent, cells were provided induction medium for two days (differentiation medium with dexamethasone, indomethacin and IBMX). Cells were then maintained in a differentiation medium until fully differentiated (day six).

METHOD DETAILS

Magnetic-activated cell sorting

BAT from 12 weeks old C57BL/6 mice was dissociated by collagenase treatment isolating unilocular adipocytes from the stromal vascular fraction (SVF). SVF was resuspended in MACS buffer (PBS, 2mM EDTA (sterile), 0.5% Bovine Serum Albumin) and sequentially incubated with Microbeads conjugated to monoclonal anti-mouse CD45 antibodies (Ly-5; isotype: rat IgG2b; clone:30F11.1, Miltenyi Biotech), monoclonal antihuman/mouse CD11b (Mac-1α) antibodies (isotype: rat IgG2b, Miltenyi Biotech).and anti-CD31 antibody (isotype: ratIgG2a, Miltenyi Biotech) or 15 min at 4°C. Finally, the $CD45^+$, $CD11b^+$ and $CD31^+$ fractions were isolated using MACS LS columns according to manufacturer instructions (Miltenyi Biotech).

ECM preparation from decellularised BAT

For each ECM preparation, 8-15 weeks-old $Lep^{Ob/Ob}$ *and* $Lep^{wt/wt}$ mice were culled, and BAT depots from each group were collected and pooled. BAT samples (around 20g) were minced and incubated in distilled water with sodium deoxycholate 0.1%, Triton X-100 0.1% and IGEPAL 0.1% for 48 h at 4°C with gentle shaking. BAT samples were then incubated in trypsin–EDTA for 4 h at 37°C with shaking and washed once with isopropanol and then twice with ethanol. After three washes with PBS, the decellularised BAT (ECM) was dialyzed overnight at 4°C against PBS. ECM was kept in sterile conditions at 4°C in PBS supplemented with fungizone (final concentration 2.5 μg/mL), penicillin (final concentration 100 UI/ml) and streptomycin (final concentration 100 μg/mL) for no more than 1 month.

Histological analysis

BAT and liver samples were fixed in 4% paraformaldehyde for 24h, embedded in paraffin, sectioned into 5 μm sections, and processed for Sirius Red/Fast green (fibrosis) or haematoxylin and eosin (H&E) staining. Sirius Red binds to all types of collagen, whereas fast green stains non-collagenous proteins. The slides were scanned using Microscopy Zeiss Axioscan Z1 Slide scanner. HALO Image Analysis Software (HALO; Indica Labs) was used to quantify liver steatosis (lipid droplet tissue area), BAT lipid droplet size, tissue/vessel area, and fibrosis. The software was optimised with specific analysis settings and was trained to identify tissue, vessels, fibrosis, damaged tissue, and glass as individual classifiers. The picrosirius staining was then quantified exclusively in the tissue and vessels classifiers, allowing for the determination of the amount of peri-AD and peri-V fibrosis and vessel area.

Immunofluorescence analysis and confocal microscopy

BAT samples and BAPs (cultured on a coverslip or in hydrogel with ECM) were fixed 30min (2D culture) or 1h (Tissue and 3D culture) in 4% paraformaldehyde for 1 h at room temperature and then transferred to PBS, in which they were stored at 4°C until immunofluorescence analysis. Samples were blocked in 1M glycine and PBS with 3% B.S.A. and 0.1% Triton X-100. Samples were then incubated with the appropriate primary antibody overnight at 4°C. Bound primary antibody was detected after 2h incubation in PBS with 3% B.S.A. using secondary antibodies conjugated to Alexa Fluor dyes (488 and 568). Neutral lipids were stained with Bodipy 493/503, and actin was stained with Alexa Fluor 546 phalloidin (Molecular Probes, Eugene, OR) during the secondary antibody incubation. Nuclei were counterstained with DAPI (Invitrogen). Samples were mounted in Fluoromount G (SouthernBiotech, Birmingham, AL, U.S.A.) and imaged blind using Zeiss LSM 510 Meta Confocal microscope with LSM 3D software (Carl Zeiss). At least three images per sample per stain were used for quantification, which was also performed blind. Images were captured and analyzed using ZEN 2009 imaging software (Carl Zeiss).

RNA extraction and real-time PCR

According to the manufacturer's instructions, RNA from BAP culture in 2D were extracted using RNeasy Mini columns (Qiagen). From frozen tissue or BAPs culture in 3D was harvested using RNA-STAT-60TM (A.M.S. Bio) and purified by chloroform extraction and isopropanol precipitation. Reverse transcription was performed using Reverse Transcriptase System (Promega) according to the manufacturer's instructions and as described in.[68] Real-time PCR was carried out using TaqMan or Sybr Green reagents using an Abi 7900 real-time PCR machine using default thermal cycler conditions and as described in.[68] Reactions were run in duplicate for each sample and quantified using the A.B.I. Prism 7900 sequence detection system (Applied Biosystems). Primer sequences are described in Table 2. Reactions were run in duplicate, checked for reproducibility, and then averaged. Duplicates were checked for reproducibility and then averaged. Product specificity was determined using a dissociation curve for SYBR green reactions. A standard curve generated from a pool of all cDNA samples was used for quantification. The expression of genes of interest was

normalised using the geometric average of four housekeeping genes (18s, 36b4, βactin, and B2m), and data are expressed as arbitrary units.

Lipolysis assay

BAPs were differentiated in 3D hydrogel with or without ECM (from $Lep^{Ob/Ob}$ and $Lep^{wt/wt}$ mice). Differentiated BAPs/hydrogels were then incubated in Krebs–Ringer bicarbonate buffer with or without NE (75 nM) for 4 h at 37°C. Glycerol was measured as an index of lipolysis by using free glycerol reagent (Sigma) against a glycerol standard curve.

Calculation of energy expenditure and maximum thermogenic capacity

Energy expenditure (EE) and Maximum thermogenic capacity (MTC) of mice were assessed by indirect calorimetry. EE was performed in-home cages in a 10-L cage and measured over 48h. MTC was performed in an oxymax calorimetry chamber with a 2.7 L capacity. For MTC, the Oxymax chamber was housed within a larger temperature-controlled cabinet. Temperature within calorimetric chambers was continuously monitored and fixed at 30°C. Oxygen consumption and carbon dioxide production were measured using a custom-built oxygen and carbon dioxide monitoring system (Creative Scientific). Airflow rates were set at 400 mL/min. EE was calculated from oxygen consumption and carbon dioxide production. Regarding MTC measurement, animals were first anesthetized under pentobarbital (60 mg/kg) anesthesia. Oxygen and carbon dioxide concentrations in room air and air, leaving each cage, were measured every 4 min. Baseline EE was taken calculated from the average of three EE measurements once a steady state was achieved (at least 3 consecutive stable measurements, usually taking ~20 min)). Mice were then injected subcutaneously with 1 mg/kg of norepinephrine bistartrate and 30 mg/kg of pentobarbital and returned to the calorimetry chamber. Energy expenditure was measured for a further 28 min. Energy expenditure was calculated from VO2 and VCO2 using a modified Weir equation. The maximal NE-stimulated energy expenditure was determined as the average of the three largest readings post injection. ANCOVA and multiple linear regression analyses were performed using SPSS 26.

QUANTIFICATION AND STATISTICAL ANALYSIS

The number of animals or independent experiments was determined based on pilot data and indicated in the figure legends. No statistical methods were used to predetermine the total number of animals needed for this study. Animal allocation to cages (4 mice/cage) and diet were not randomised as we ensured each cage had mice from the two genotypes and each group (chow and HFD) had the same average of initial body weight. While blinded during the experiments and assessment of the outcome, the investigators were not blinded to the animals' allocation. Mice were divided into groups with the same average body weight per group. All data from experiments are summarised by their mean, with error bars showing the standard error of the mean. The number of replicates is reported in the figure legends. When the pairwise comparison results are expressed as a fold-change, it is declared in the figure legends to what value the data were normalised. Statistical analyses and Grubbs'tests to exclude outliers were performed using Prism8 (GraphPad). Comparisons between two independent groups were conducted using an unpaired t test or Mann Whitney U-test in the case of non-normally distributed datasets. Comparison between more than two groups was performed using a one-way ANOVA followed by appropriate post hoc multiple comparisons tests. Comparisons between more than two groups and factors were conducted using a two-way ANOVA followed by appropriate post hoc testing. Pearson's or Spearman's coefficients were evaluated to estimate the extent of correlation between data series. Correlation matrix analysis was performed using Prism8 and R-studio. Hierarchical clustering was performed using ClustVis web-tool.[69] Data points were excluded from the correlation analysis if they exhibited a value of more than two S.D.s from the mean. Statistical significance was set at $p < 0.05$.